Toys for quantum computation

Aard Keimpema

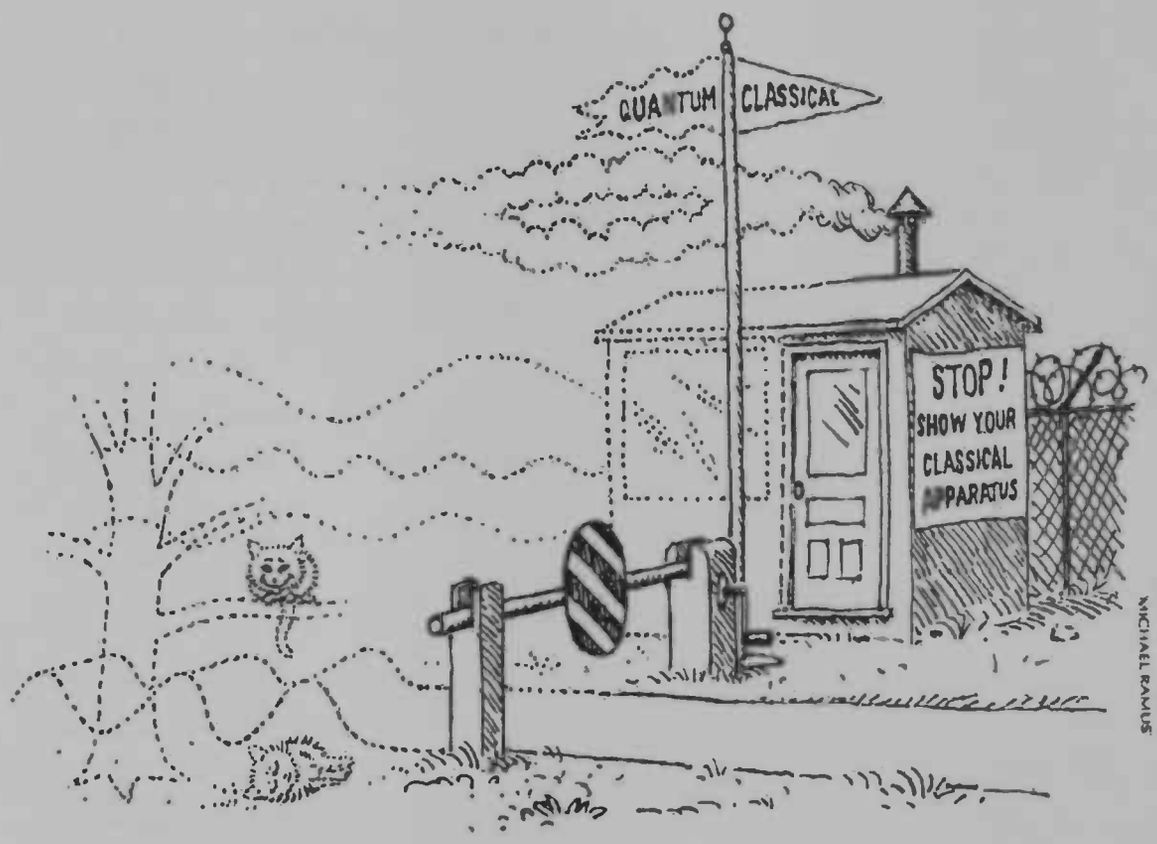

Contents

Introduction

A formal definition of a quantum computer would be that it is a system whose quantum mechanical time evolution is used to do computation. A quantum computer just like an classical computer has the bit as unit of information, in the context of quantum computation called a qubit. Because a quantum computer operates in the quantum mechanical domain, a collection of qubits can hold not one value but a superposition of many values. This "quantum parallelism" is a fundamental advantage that a quantum computer has over a classical computer and algorithms that exploit this feature can be significantly faster than any classical algorithm. That said, the number of algorithm available today is small and their usefulness is limited. Several hardware implementations of quantum computers have been made. Unfortunately existing quantum hardware technology limits the size of these experimental quantum computers to just a few qubits. In chapter 1 we review the field of quantum computation and introduce an interesting new hardware candidate, dubbed the "quantum toy" by its creators. This quantum toy is a metallic ring with three embedded ferromagnets. In certain configurations these ferromagnets can induce a current in the ring. In fact the configurations that will or will not induce a current can be identified with an CNOT(XOR) gate. This motivates us to explore the viability of this system using computer simulations.

The quantum toy system is related to a long standing problem in condensed matter physics, that of the persistent currents. When a small metal ring is placed in a static magnetic field, the magnetic field will induce a current in the ring. Persistent currents have been observed experimentally and a great discrepancy between theory and experiment was found. The qualitative features of the phenomenon are explained well by theory, but the size of the current measured was one to two orders of magnitude larger then that predicted by experiment. As a second object of this master thesis we will study persistent current numerically using a simple tight-binding model and compare this to existing theory and experiment. In chapter two we review the field of persistent currents and we give an overview of existing theory.

To make a simulation tool of a quantum mechanical system basically means that we have to solve the Schrödinger equation numerically. In chapter 3 we briefly discuss two such method, namely the Cranck-Nicholson method and the Suzuki-Trotter method. We will use the latter in our simulation tool. The actual simulation is described in chapter 4. In this chapter we detail the development of the numerical tool and show its correctness at each step. We find that the simulations qualitatively show the same features as we would expect theoretically and experimentally. The size of current is a different matter. When compared to experiment we find that although our results are of the same order of magnitude we cannot make an accurate fit to the experimental data using our simple model.

In the last chapter we investigate the properties of the quantum toy system by computer simulations. We will explore its application for quantum computation and its use as a measurement device. Upon investigating how a quantum toy system can be used in a quantum circuit, we find that the quantum toy is not useful for quantum computation. We then focus on the second application, that of a measurement device. The idea being that we can exploit the dependence of the induced current to the direction of the embedded ferromagnets. To verify if such a scheme will work, we need to investigate if we can

reproduce the theoretical values of the induced current. We found major discrepancies between theory and our simulations. We found for instance that the induced current has an erratic dependence on the electron density.

We then split our investigation between the single electron case and the half-filled case found in most metals. The single electron case only matches the theory qualitatively. We find that indeed such a single electron system can be build and be used as a measurement device. In the half-filled case we find that the dependence of the current on the various parameters is so erratic that we conclude that according to our simulations, a metallic quantum toy could not be used as a measurement device. An explanation for the difference between theory and our simulations could unfortunately not be found. To investigate this we would have to repeat the original calculations, which is outside the scope of this master thesis.

Chapter 1

Introduction to quantum computation

1.1 Introduction

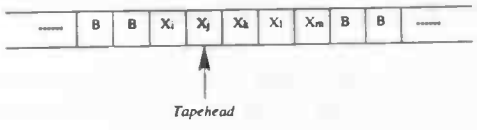

Figure 1.1: *The input tape of a Turing machine.*

The classical computer which we know today is based on the so called Turing machine[1], named after its inventor the English mathematician Alan Turing. A Turing machine(TM) is an automata which reads its input from a tape. This tape is divided into cells and in each cell there is one input symbol, this is illustrated in Fig. 1.1. Suppose the TM is in a state α, upon reading a symbol Γ the TM invokes a transition function $\delta(\alpha, \Gamma)$. The transition function determines according to the current state α and the input symbol Γ the next state β the TM shall move to. Also the current symbol on the tape is changed to some symbol Σ and the tape head is moved one cell to the left or the right. The computation ends when the TM enters an accepting state. Formally a TM is represented by a 7-tuple

$$M = (Q, \Sigma, \Gamma, \delta, q_0, B, F), \tag{1.1}$$

where

- Q is the set of states of the TM,
- Σ is the set of input symbols,
- $\Gamma \subset \Sigma$ is the set of tape symbols,
- $\delta(q, X) = (p, Y, D)$ is the transition function, that takes the TM from the state q to the state p upon reading the symbol $X \in \Gamma$ and replaces X on the tape with some $Y \in \Gamma$. The tape head then moves one place in the direction D which is either left or right,
- q_0 is the start state,
- $B \notin \Sigma$ is the blank symbol, this signifies that a tape cell does not contain a symbol,
- $F \subset Q$ is the set of accepting states.

The importance of the turing machine lies in the (unproven) Church-Turing thesis: [2][1],

Theorem 1 (Church-Turing) *Every 'function which would naturally be regarded as computable' can be computed by the universal Turing machine.*

The notion "naturally computable" is best explained by stating when a function is not "naturally computable". A function is not "naturally computable" when either the TM fails to reach an accepting state (the problem is undecidable) or the computing time grows exponentially with the size of the input (the problem is intractable). The Church-Turing theorem reduces the question if a problem is solvable to the question "can the problem be solved on a TM in linear time".

The TM the way it was proposed by Turing is based on a classical picture. Can it be used to solve a quantum mechanical problem? Richard Feynman in his classical paper[3] answered this question. He concluded that a classical computer is not able to simulate a quantum mechanical problem (exactly) in the Church-Turing sense. The storage requirements and the computation time for such a simulation grows exponentially with the size of the system. Feynman showed that the only class of computers that would be able to simulate a quantum mechanical system is as he puts it "a computer which itself is build of quantum mechanical elements which obey quantum mechanical laws". David Deutsch expressed this fact in his reformulation of the Church-Turing theorem[4]:

Theorem 2 (The Church-Turing-Deutsch principal) *Every finitely realizable physical system can be perfectly simulated by a quantum computer operating by finite means.*

This is in essence a physical reformulation of the Church-Turing theorem. But because as Feynman showed a classical computer cannot simulate a non trivial quantum mechanical system exactly in the Church-Turing sense, it is more restrictive.

The most logical way to build a theoretical model for a quantum computer(QC) is to design a quantum version of the TM. This is the approach initially taken by Deutsch[4]. A more intuitive approach, also due to Deutsch, is by using a quantum circuit model[5]. This has been shown to be equivalent to a quantum TM[7]. The quantum circuit model works in a similar manner like a normal electrical circuit except the wires now represent qubits and all the logic gates are replaced by unitary quantum gates.

Arguably the most important gate is the controlled-NOT (CNOT) gate. The CNOT gate has two inputs, a control bit and a target bit. If the control bit is '1' then the target bit is inverted. Otherwise it is left unchanged. In Table 1.1 the truth table is given. Note that the first bit is the *leftmost* digit (unlike the standard computer science convention which takes the rightmost digit as the first bit). In Fig. 1.2 its circuit representation is given. The reason why CNOT is important is that together with some arbitrary single qubit gates it can used to produce any other quantum gate. This is similar to the NAND gate in classical computing which is sufficient to build any classical logic gate. We will postpone further discussion of quantum gates to the next section.

$\|in\rangle$	$\|out\rangle$
$\|00\rangle$	$\|00\rangle$
$\|01\rangle$	$\|01\rangle$
$\|10\rangle$	$\|11\rangle$
$\|11\rangle$	$\|10\rangle$

Table 1.1: *Truth table of* CNOT, *the leftmost qubit is the control qubit and the rightmost qubit is the target qubit.*

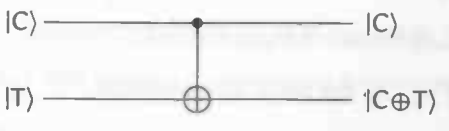

Figure 1.2: *Circuit representation of* CNOT, *where* $|C\rangle$ *is the controll qubit and* $|T\rangle$ *the target qubit.*

Simulating quantum mechanics is by itself an interesting application, but it is not the primary reason why quantum computation is getting wide attention. There are algorithms which are fundamentally faster (are of lower order) for their specific task than any classical algorithm. An example is Grover's algorithm[8, 9] which can search a database using $O(\sqrt{N})$ operations, while classically at least O(N)

operations are needed. Unfortunately there are few useful quantum algorithms known and after the mid-1990'ties no new useful algorithms were found. In section 1.3 we will explore the subject of quantum algorithms further.

1.2 Quantum Gates

1.2.1 Single qubit operations

Consider an arbitrary single qubit state,

$$\psi = \alpha \begin{pmatrix} 1 \\ 0 \end{pmatrix} + \beta \begin{pmatrix} 0 \\ 1 \end{pmatrix} = \alpha|0\rangle + \beta|1\rangle, \tag{1.2}$$

where α and β are complex constants, with the condition $\alpha^2 + \beta^2 = 1$. A single qubit can be thought of in terms of a 3-dimensional vector representation analogous to the vector representation of a spin. The spin up component of the state vector in this analogy is α and the spin down component is β. This is illustrated in Fig. 1.3.

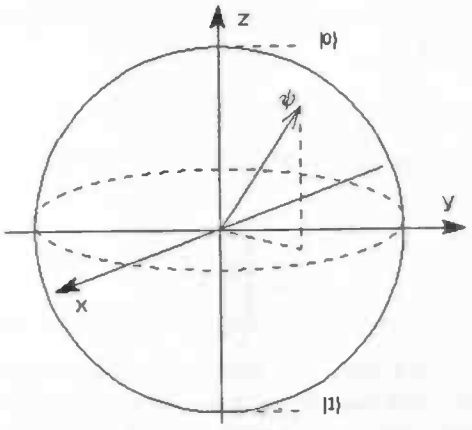

Figure 1.3: *Vector representation of a single qubit.*

A single qubit gate performs some linear (unitary) transformation on the state vector. An obvious example of a linear transformation is a rotation. Especially important rotations for quantum computation (as we shall see later) are the rotations of $\pi/2$ degrees around the $\hat{x}$, $\hat{y}$ and $\hat{z}$ direction. To perform these rotations we need the Pauli spin matrices

$$\sigma_x \equiv \begin{pmatrix} 0 & 1 \\ 1 & 0 \end{pmatrix}, \qquad \sigma_y \equiv \begin{pmatrix} 0 & -i \\ i & 0 \end{pmatrix}, \qquad \sigma_z \equiv \begin{pmatrix} 1 & 0 \\ 0 & -1 \end{pmatrix}. \tag{1.3}$$

A rotation about ϕ degrees around the α axis is performs by multiplying the state vector with $e^{i\hbar\phi\sigma_\alpha/2}$. Let X be the rotation operator that rotates the state vector around $\pi/2$ degrees around the $\hat{x}$ axis (and similarly Y and Z for the $\hat{y}$ and the $\hat{z}$ directions), the operators are given by

$$X \equiv \frac{1}{\sqrt{2}} \begin{pmatrix} 1 & i \\ i & 1 \end{pmatrix}, \qquad Y \equiv \frac{1}{\sqrt{2}} \begin{pmatrix} 1 & 1 \\ -1 & 1 \end{pmatrix}, \qquad Z \equiv \frac{1}{\sqrt{2}} \begin{pmatrix} 1+i & 0 \\ 0 & 1-i \end{pmatrix}. \tag{1.4}$$

Similarly the inverse rotations of $-\pi/2$ degrees $\bar{X}$, $\bar{Y}$ and $\bar{Z}$ can be constructed by taking the complex conjugate. From these gates we can construct other gates, e.g. a not gate can be build by applying X (or Y) two times. Also we can build each rotation from the other two rotations, e.g. $Z = \bar{Y}XY = \bar{X}YX$.

Another important gate which is often used in quantum algorithms is the Hadamard gate. It is given by

$$H \equiv \frac{1}{\sqrt{2}} \begin{pmatrix} 1 & 1 \\ 1 & -1 \end{pmatrix}. \tag{1.5}$$

The Hadamard gate is nothing more than Y followed by a reflection in the $\hat{x} - \hat{y}$ plane, its circuit is given in Fig. 1.4.

Figure 1.4: *The Hadamard gate.*

The Hadamard gate can be used to create uniform superpositions. For instance two qubits can be put an uniform superposition state of all possible combinations of those qubits. This is achieved by putting both qubits in the state $|0\rangle$ and then performing an Hadamard transformation on both qubits. This will produce a state

$$\psi = \frac{|00\rangle + |10\rangle + |01\rangle + |11\rangle}{2}. \tag{1.6}$$

1.2.2 Multi qubit operations

The two qubit state vector is given by

$$\psi = \alpha|00\rangle + \beta|10\rangle + \gamma|01\rangle + \rho|11\rangle, \tag{1.7}$$

or more conveniently in a vector

$$\psi = \begin{pmatrix} \alpha \\ \beta \\ \gamma \\ \rho \end{pmatrix}. \tag{1.8}$$

Higher qubit cases are constructed similarly. The order of the basis states in the state vector is just the normal binary ordering (note again that the first bit is the *leftmost* bit). Thus for a three qubit state vector the first element is $|000\rangle$, the second $|100\rangle$, ending with $|111\rangle$ as the last element.

Multi-qubit gates are conceptually different from single qubit gates in that they represent some kind of interaction between qubits. This interaction makes the multi-qubit case much more complex than the single qubit case. The interaction between two qubits i and j is performed with the controlled phase shift operator

$$I_{ij} \equiv \begin{pmatrix} e^{i\phi_{00}} & 0 & 0 & 0 \\ 0 & e^{i\phi_{10}} & 0 & 0 \\ 0 & 0 & e^{i\phi_{01}} & 0 \\ 0 & 0 & 0 & e^{i\phi_{11}} \end{pmatrix}, \tag{1.9}$$

which gives a phase shift depending on the state of both qubits and thus realizing an interaction.

In the introduction we introduced the CNOT gate and noted that it was a fundamental gate. In matrix form the CNOT gate becomes

$$\text{CNOT} \equiv \begin{pmatrix} 1 & 0 & 0 & 0 \\ 0 & 1 & 0 & 0 \\ 0 & 0 & 0 & 1 \\ 0 & 0 & 1 & 0 \end{pmatrix}. \tag{1.10}$$

We can build a CNOT gate using the gates introduced up to this point, if we group CNOT in 2×2 blocks we can write it as

$$\text{CNOT} \equiv \begin{pmatrix} I & 0 \\ 0 & \sigma_x \end{pmatrix} = \begin{pmatrix} I & 0 \\ 0 & \bar{Y}\sigma_z Y \end{pmatrix} = \bar{Y} \begin{pmatrix} I & 0 \\ 0 & \sigma_z \end{pmatrix} Y = \bar{Y} I_{12} Y, \tag{1.11}$$

with I the identity matrix, $\phi_{00} = \phi_{10} = \phi_{01} = 0$ and $\phi_{11} = \pi$.

Another useful gate is the Toffoli gate which is similar to the CNOT gate. It is a three qubit gate with two control bits and one target bit. The target bit is inverted when both control bit are $|1\rangle$ otherwise it is left unchanged. In Table 1.2 the truth table of the gate is given and in Fig. 1.5 the circuit representation is shown.

In	Out
$\|000\rangle$	$\|000\rangle$
$\|100\rangle$	$\|100\rangle$
$\|010\rangle$	$\|010\rangle$
$\|110\rangle$	$\|111\rangle$
$\|001\rangle$	$\|001\rangle$
$\|101\rangle$	$\|101\rangle$
$\|011\rangle$	$\|011\rangle$
$\|111\rangle$	$\|110\rangle$

Table 1.2: *Truth table of the Toffoli gate*

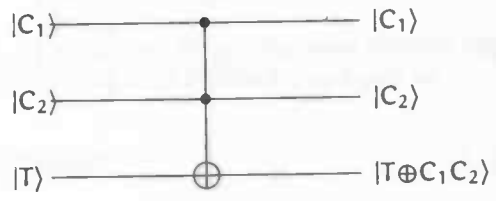

Figure 1.5: *Circuit representation of the Toffoli gate*

Note that the Toffoli gate is quite similar to the classical AND gate, in fact we can use it to reproduce the classical NAND gate as illustrated in Fig. 1.6. Because NAND is a fundamental gate in classical computing, the Toffoli gate can be used to reproduce any classical algorithm on a QC.

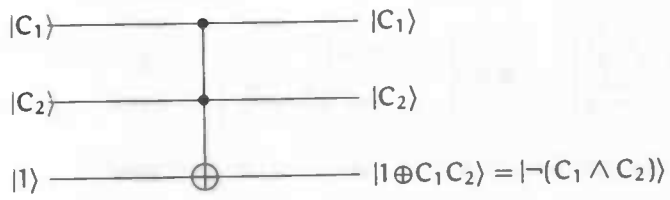

Figure 1.6: *Classical* NAND *gate constructed with a Toffoli gate*

Consider some arbitrary function $f(x)$, suppose we want to incorporate it in a quantum circuit. For this there exists the U_f gate which takes two inputs $|x\rangle$ and $|y\rangle$ and outputs $|y \oplus f(x)\rangle$. The circuit for this gate is[1]

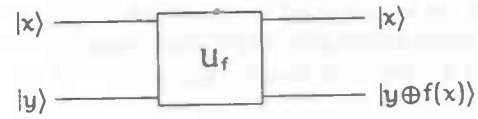

Figure 1.7: *The U_f gate for an arbitrary function $f(x)$*

1.3 Quantum Algorithms

1.3.1 The Deutsch-Josza algorithm

The oldest quantum algorithm which is fundamentally faster than any classical algorithm is Deutsch's algorithm. Unfortunately the algorithm itself is not very useful, its importance lies more in the fact that is a proof of concept. Deutsch's algorithm[4] is an application of quantum parallelism, consider an

[1] Note that in this context $|x\rangle$ and $|y\rangle$ can contain more then one qubit.

arbitrary function $f(x) : \{0,1\} \rightarrow \{0,1\}$. Note that there are 4 possible functions in this case: Constant 0, constant 1, the identity and the inverse function (defined by $f(0) = 1$ and $f(1) = 0$).

Suppose we were interested to determine if the function $f(x)$ is constant. Classically this requires two evaluations of $f(x)$, but Deutsch's algorithm allows it to be computed in one evaluation. The network of Deutsch's algorithm is given in Fig. 1.8.

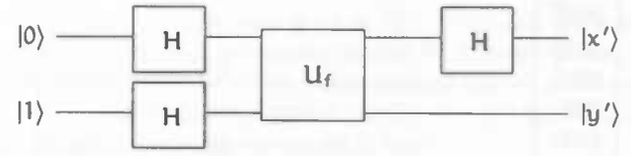

Figure 1.8: *Deutsch's algorithm*

In the first step of the algorithm we put both qubits in a mixed state using the Hadamard gate

$$|\psi\rangle = \left[\frac{|0\rangle_1 + |1\rangle_1}{\sqrt{2}}\right]\left[\frac{|0\rangle_2 - |1\rangle_2}{\sqrt{2}}\right], \tag{1.12}$$

applying U_f to this state gives after some simple algebra,

$$\psi = \begin{cases} |\psi\rangle = \pm\left[\frac{|0\rangle_1 + |1\rangle_1}{\sqrt{2}}\right]\left[\frac{|0\rangle_2 - |1\rangle_2}{\sqrt{2}}\right] & \text{if } f(0) = f(1) \\ |\psi\rangle = \pm\left[\frac{|0\rangle_1 - |1\rangle_1}{\sqrt{2}}\right]\left[\frac{|0\rangle_2 - |1\rangle_2}{\sqrt{2}}\right] & \text{if } f(0) \neq f(1), \end{cases} \tag{1.13}$$

the final Hadamard transformation then gives our final result

$$\psi = \begin{cases} |\psi\rangle = \pm|0\rangle_1\left[\frac{|0\rangle_2 - |1\rangle_2}{\sqrt{2}}\right] & \text{if } f(0) = f(1) \\ |\psi\rangle = \pm|1\rangle_1\left[\frac{|0\rangle_2 - |1\rangle_2}{\sqrt{2}}\right] & \text{if } f(0) \neq f(1), \end{cases} \tag{1.14}$$

upon measurement of the first qubit we now know in one measurement if $f(x)$ is constant or not.

Now we extend Deutsch's algorithm to n qubits, we define a function $f(x) : \{0,1\}^n \rightarrow \{0,1\}$ which is either constant or a balanced function (balanced means that in 50% of the cases the function returns a '0' and in the other 50% a '1'). If we would want to investigate if the function is balanced or constant then classically we would, in the worst case, need $n/2 + 1$ evaluations of $f(x)$. There exists an generalization of Deutsch's algorithm called the Deutsch-Josza[6] algorithm that can determine this in one evaluation. Its network is given in Fig. 1.9.

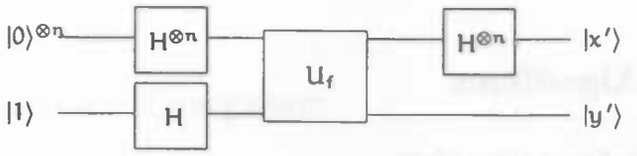

Figure 1.9: *The Deutsch-Jozsa algorithm.*

In the first step of the algorithm the top n qubits are put in a superposition state containing all possible combinations with equal probability. This application of the Hadamard gate was demonstrated in the

previous section. We obtain a state a state

$$\psi = \left[\frac{|00..0\rangle + |10..0\rangle + \cdots + |11..1\rangle = \sum_{x=0}^{2^n-1}|x\rangle}{\sqrt{2^n}}\right]\left[\frac{|0\rangle - |1\rangle}{\sqrt{2}}\right], \tag{1.15}$$

where we omit the qubit labels as it is understood to which qubits each term applies. Applying U_f gives

$$\psi = \left[\sum_{x=0}^{2^n-1}\frac{(-1)^{f(x)}|x\rangle}{\sqrt{2^n}}\right]\left[\frac{|0\rangle - |1\rangle}{\sqrt{2}}\right]. \tag{1.16}$$

In the final step the top n qubits are again put through a Hadamard gate. This is the most difficult step to follow. We will show this operation in detail. First we write the effect of the Hadamard gate as

$$H|x\rangle = \frac{1}{\sqrt{2^n}}\sum_{y=0}^{2^n-1}(-1)^{x\cdot y}|y\rangle. \tag{1.17}$$

This notation is best understood by an example, consider the case $n = 1$

$$H|0\rangle = \frac{(-1)^{0\cdot 0}|0\rangle + (-1)^{0\cdot 1}|1\rangle}{\sqrt{2}} = \frac{|0\rangle + |1\rangle}{\sqrt{2}}, \qquad H|1\rangle = \frac{(-1)^{1\cdot 0}|0\rangle + (-1)^{1\cdot 1}|1\rangle}{\sqrt{2}} = \frac{|0\rangle - |1\rangle}{\sqrt{2}}. \tag{1.18}$$

The effect of the Hadamard gate on n qubits is thus

$$\begin{aligned} H|x\rangle = [H|x_1\rangle]\,[H|x_2\rangle]\cdots[H|x_n\rangle] &= \frac{1}{\sqrt{2^n}}\left[\sum_{y_1=0}^{2^n-1}(-1)^{x_1\cdot y_1}|y_1\rangle\right]\left[\sum_{y_2=0}^{2^n-1}(-1)^{x_2\cdot y_2}|y_2\rangle\right]\cdots\left[\sum_{y_n=0}^{2^n-1}(-1)^{x_n\cdot y_n}|y_n\rangle\right] \\ &= \frac{1}{\sqrt{2^n}}\sum_{y=0}^{2^n-1}(-1)^{x\cdot y}|y\rangle. \end{aligned} \tag{1.19}$$

Applying this result to (1.16) gives

$$\psi = \left[\sum_{x=0}^{2^n-1}\frac{(-1)^{f(x)}H|x\rangle}{\sqrt{2^n}}\right]\left[\frac{|0\rangle - |1\rangle}{\sqrt{2}}\right] = \left[\sum_{x=0}^{2^n-1}\sum_{y=0}^{2^n-1}\frac{(-1)^{f(x)}(-1)^{x\cdot y}|y\rangle}{2^n}\right]\left[\frac{|0\rangle - |1\rangle}{\sqrt{2}}\right]. \tag{1.20}$$

Now suppose that $f(x)$ is a constant function, then we can move the term $(-1)^{f(x)}$ outside of the sum. We fix $|y\rangle$ at some non-zero value, then the sum

$$\sum_{x=0}^{2^n-1}\frac{(-1)^{x\cdot y}|y\rangle}{2^n} = 0, \qquad (|y\rangle \neq |0\rangle) \tag{1.21}$$

because the factor $(-1)^{x\cdot y}$ will just as often negative as it will be positive. The only $|y\rangle$ state which will survive is $|0\rangle$.

Now suppose that $f(x)$ is a balanced function and that $|y\rangle = |0\rangle$. Then the wave function will vanish because

$$\sum_{x=0}^{2^n-1}\frac{(-1)^{f(x)}(-1)^{x\cdot 0}|0\rangle}{2^n} = 0, \tag{1.22}$$

thus if $f(x)$ is balanced $|y\rangle$ will never be in the state $|0\rangle$. Now lets summarize our result, if $|y\rangle = |0\rangle$ then $f(x)$ is constant, if $|y\rangle$ is in any other state than $|0\rangle$ then $f(x)$ is balanced. Although this algorithm has no practical application it is a nice proof of concept that can be used as a test case for a physical QC.

1.4 Decoherence

Quantum computation relies on the fact that a quantum mechanical state can be in an arbitrary superposition of all possible states. In the classical world, we know from everyday life that these superposition states are never observed. But if nature is described by quantum mechanics then why do these superposition states not exist in the classic world of everyday life? This problem is closely related to the measurement problem due to von Neumann[10].

Suppose we have some spin-$\frac{1}{2}$ system in a state $\psi = \alpha|\uparrow\rangle + \beta|\downarrow\rangle$ and we want to do a measurement on this state using a quantum mechanical measuring device M. The device can either be in a state $|M_\uparrow\rangle$ or $|M_\downarrow\rangle$. Furthermore there is a mechanism in the measurement device so that when the system is spin down the measurement device makes the transition $|\downarrow\rangle|M_\uparrow\rangle \rightarrow |\downarrow\rangle|M_\downarrow\rangle$. Initially we will put M in the state $|M_\uparrow\rangle$ The state of the system after a measurement is thus

$$|\Phi\rangle = \alpha|\uparrow\rangle|M_\uparrow\rangle + \beta|\downarrow\rangle|M_\downarrow\rangle. \tag{1.23}$$

If we write the density matrix ρ of this system,

$$\rho = |\Phi\rangle\langle\Phi| = |\alpha|^2|\uparrow\rangle\langle\uparrow|M_\uparrow\rangle\langle M_\uparrow| + |\beta|^2|\downarrow\rangle\langle\downarrow|M_\downarrow\rangle\langle M_\downarrow| + \alpha\beta^*|\uparrow\rangle\langle\downarrow|M_\uparrow\rangle\langle M_\downarrow| + \beta\alpha^*|\downarrow\rangle\langle\uparrow|M_\downarrow\rangle\langle M_\uparrow|. \tag{1.24}$$

In the classical limit we need to discard the off-diagonal terms of the density matrix. Von Neumann introduced for this a non unitary process, which he dubbed "process 1" that kills all coherences. The result of "process 1" leaves us with the reduced density matrix

$$\rho^\tau = |\alpha|^2|\uparrow\rangle\langle\uparrow|M_\uparrow\rangle\langle M_\uparrow| + |\beta|^2|\downarrow\rangle\langle\downarrow|M_\downarrow\rangle\langle M_\downarrow|, \tag{1.25}$$

where $|\alpha|^2$ and $|\beta|^2$ are probabilities. Of course the question remains, what is the origin of this "process 1". The solution comes from the fact that the Schrödinger equation describes the unitary evolution of a *closed* system, but in fact no quantum system is closed as every system will interact with its environment. In informal language the information contained in the coherences is leaked into the environment.

To model the process of decoherence we use the master equation,

$$\dot{\rho}_{n,m} = -\frac{i}{\hbar}[H,\rho]_{n,m} - \gamma_{n,m}(\rho_{n,m} - \rho^{eq}_{n,m}), \text{ with } \rho^{eq}_{n,m} = 0 \text{ for } n \neq m \tag{1.26}$$

with $\rho^{eq}_{n,m}$ the equilibrium value and γ a phenomenological damping term describing the decay of the coherences induced by "process 1", γ is known as the dephasing rate [2]. The derivation of equation (1.26) is fairly straightforward. The first term comes from the actual differentiation of the density matrix whereas the second term is added to model the decay of the coherences (which after all doesn't come from Schrödingers equation).

The importance of the dephasing rate in the context of quantum computation is that it gives a time limit within which an algorithm can operate. This time limit greatly complicates the development of a physical quantum computer.

1.5 Physical Quantum Computers

To build a physical QC is far from straightforward. In fact the largest quantum computer build to date had only seven qubits [11]. There are many proposals of candidates for QC hardware. We will now discuss some of these candidates candidates. For a more complete review see Ref. [16].

[2] In the case when the process that we are describing is a decay process we have $\gamma_{n,m} = \gamma^{deph}_{n,m} + \frac{1}{2}(\Gamma_n + \Gamma_m)$ where Γ_n and Γ_m describe the decay rates from state n respectively m

1.5.1 Nuclear Magnetic Resonance

The NMR QC is the most simple QC to realize experimentally and as such it is the type of QC that is most often used in experiment. The scheme is simple. We use the spins of nuclei as qubits. Each nucleus will have a slightly different magnetic moment. By applying a magnetic field tuned to the resonance frequency of a particular nucleus we can rotate the spins individually. In a typical setup the spins are contained in some (complex) molecule. An experiment is then carried out over some ensemble of typically 10^{20} molecules.

The most famous experimental realization of a NMR QC was done at IBM by Vandersypen et al. [11], they did an experimental realization of Shor's algorithm on a seven qubit NMR QC (as mentioned previously this is the record amount of qubits to date).

Unfortunately the NMR QC has one major problem. Because all spins are in the same molecule it is very difficult to build a setup containing more then a few qubits. Unless a scheme is invented that does away with the need for these complex molecules, it seems very unlikely that a NMR QC can be useful for computation. But even in its current form the NMR QC is important as a proof of concept and can be used as a testbed for quantum algorithms.

1.5.2 Ion traps

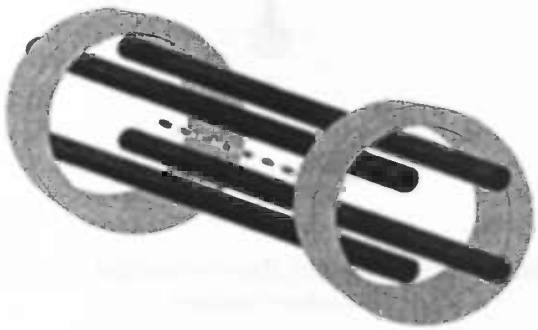

Figure 1.10: *An ion trap known as the linear Paul trap. On the electrodes an RF field is applied trapping the enclosed ions in the radial direction, on the end rings an dc field is applied confining the ions the longitudinal direction.*

An ion trap QC is a scheme in which a series of ions is trapped inside a linear Paul trap[12, 13][3]. The ions are also cooled to lower decoherance. In figure 1.10 a linear Paul traps is shown. On the electrodes there is a RF field applied. At the right frequency this field gives a net central force with the origin in the center of the trap. This traps the ions in the radial direction. Furthermore at the end there are two rings to which a static field is applied. This confines the ions in the longitudinal direction.

The actual computation is done as follows[14]: We assume that there are two long lived states $|g\rangle$ and $|e\rangle$. These state constitute a qubit. Also we consider the first two collective vibrational modes $|0\rangle$ and $|1\rangle$ of the ions. We can excite the ions using laser pulses. As an example we will now demonstrate how a controlled Z gate can be build on a ion-trap QC using two ions a and b. Suppose that initially the two qubit system is in the vibrational ground state $|0\rangle$. First we give a laser pulse to ion a with the effect

$$\begin{aligned} |g\rangle_a|0\rangle &\rightarrow |g\rangle_a|0\rangle, \\ |e\rangle_a|0\rangle &\rightarrow |g\rangle_a|1\rangle. \end{aligned} \tag{1.27}$$

[3] As a side note, Wolfgang Paul received a Nobel prize for his ion trap in 1989 together with Hans Dehmelt and Norman F. Ramsey.

Then a second pulse on ion b is applied with the effect

$$\begin{aligned} |g\rangle_b|0\rangle &\rightarrow |g\rangle_b|0\rangle, \\ |g\rangle_b|1\rangle &\rightarrow |g\rangle_b|1\rangle, \\ |e\rangle_b|0\rangle &\rightarrow |e\rangle_b|0\rangle, \\ |e\rangle_b|1\rangle &\rightarrow -|e\rangle_b|1\rangle, \end{aligned} \tag{1.28}$$

after which the first pulse to ion a is repeated, leading to a total effect

$$\begin{aligned} |g\rangle_a|g\rangle_b|0\rangle &\rightarrow |g\rangle_a|g\rangle_b|0\rangle, \\ |g\rangle_a|e\rangle_b|0\rangle &\rightarrow |g\rangle_a|e\rangle_b|0\rangle, \\ |e\rangle_a|g\rangle_b|0\rangle &\rightarrow |e\rangle_a|g\rangle_b|0\rangle, \\ |e\rangle_a|e\rangle_b|0\rangle &\rightarrow -|e\rangle_a|e\rangle_b|0\rangle, \end{aligned} \tag{1.29}$$

which is just the controlled Z gate. An example of an experimental realization of a ion-trap QC is the experiment done by Gulde et al.[15] who have realized the Deutsch-Josza algorithm on a 3 qubit ion-trap QC.

1.5.3 The quantum toy

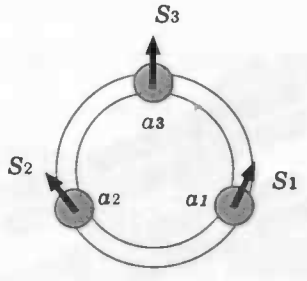

Figure 1.11: *The quantum toy, a metallic ring with three embedded ferromagnets, here* S_i *is the magnetization direction*

A promising candidate for QC hardware was recently proposed by Tatara and Garcia[2], this system dubbed "the quantum toy" is shown in Fig. 1.11. The details of this system are postponed to chapter 5. But as this system serves as a motivation for the rest for the rest of the thesis, will now give a short description. The quantum toy is a small metal ring which has three ferromagnets embedded, labeled S_1, S_2 and S_3. These ferromagnets can in the right configuration induce a current in the ring. In fact the current I in the ring has the following proportionality

$$I \propto S_1 \cdot (S_2 \times S_3). \tag{1.30}$$

This product is only non-zero if none of the ferromagnets are parallel to each other. Suppose now that we fix S_1 in the $\hat{z}$ direction and restrict the other two magnets to the $\hat{x} - \hat{y}$ plane. These two magnets will be our qubits, we assign the value 0 to the $\hat{x}$ direction and assign 1 to the $\hat{y}$ direction. Below we have constructed a truth table for this arrangement. The truth table is just that of a CNOT(XOR) gate, which is a fundamental gate for quantum computation as we saw previously in this chapter.

S_2	S_3	I
0	0	0
0	1	1
1	0	-1
1	1	0

Table 1.3: *Truth table of* $I = \hat{z} \cdot (S_2 \times S_3)$, *with* $0 = \hat{x}$ *and* $1 = \hat{y}$.

This system seems very promising and it will be one of the goals of this master thesis to study the viability of this system by means of computer simulation. Besides quantum computation, the quantum toy is also of interest because it is related to a major problem in mesoscopic physics, namely that of the persistent currents. We will discuss persistent current in detail in the next chapter.

1.6 Conclusion

The fact that there exist quantum algorithms that are fundamentally faster then any classical algorithm suggest that in the future quantum computation might be able to offer tremendous performance increases in certain applications. Presently a number of experiments were done on various QC hardware implementations (most notably using NMR and ion trap technologies). Unfortunately these systems will not scale up to more then a few bits. What is lacking at present is a viable QC hardware that can be made large enough to be useful for actual computations. The recently proposed quantum toy system [2] seems to be a promising candidate. It will be one of the goals of this thesis to study this system using computer simulations.

Bibliography

[1] A. Turing, *"On Computable Numbers with an Application to the Entscheidungsproblem"*, Proc. London Math. Society **42**, 230(1936).

[2] A. Church, *"An unsolvable problem of elementary number theory"*, American J. Math. 58, 345(1936).

[3] R. Feynman, *"Simulating physics with computers"*, Int. J. Theor. Phys. **21**, 467(1982).

[4] D. Deutsch, *"Quantum computers and the Church-Turing principle"*, Proc. R. Soc. Lond. **A400**, 97(1985).

[5] D. Deutsch, *"Quantum Computational Networks"*, Proc. R. Soc. Lond. **A425**, 73(1989).

[6] D. Deutsch and R. Jozsa, *"Rapid solutions of problems by quantum computation"*, Proc. R. Soc. Lond. **A439**, 553(1992).

[7] A.C.C. Yao, *"Quantum circuit complexity"*, Proc. of the 34th IEEE Symposium on Foundations of Computer Science, 352(1993), `http://citeseer.nj.nec.com/yao93quantum.html`.

[8] L.K. Grover, *"A fast quantum mechanical algorithm for database search"*, Proc. 28th Annual ACM Symposium on the Theory of Computation, 212(1996), `http://arxiv.org/abs/quant-ph/9605043` (revised version).

[9] L.K. Grover, *"Quantum Mechanics Helps in Searching for a Needle in a Haystack"*, Phys. Rev. Lett. **79**, 325(1997), `http://arxiv.org/abs/quant-ph/9706033`.

[10] J. von Neumann, *"Mathematische Grundlagen der Quantenmechanik"*, Springer Verlag (1932).

[11] L.V.M. Vandersypen, M. Steffer, G. Breyta, C.S. Yannoni, M.H. Sherwood and I.L. Chuang, *"Experimental realization of Shor's quantum factoring algorithm using nuclear magnetic resonance"*, Nature **414**, 883(2001).

[12] W. Paul, H.P. Reinhard and U. von Zahn, *"The electric mass filter as mass spectrometer and isotope separator"*, Z. Physik **152**(1958), p143.

[13] J.D. Prestage, G.J. Dick and L. Maleki, *"New ion traps for frequency standard applications"*, J. Appl. Phys. 66, 1013(1989).

[14] J.I. Cirac and P. Zoller, *"Quantum Computation with Cold Trapped Ions"*, Phys. Rev. Lett. **74**, 4091(1995).

[15] S. Gulde, M. Riebe, G. T. Lancaster, C. Becher, J. Escher, H. Häfnner, F. Schmidt-Kaler, I. L. Chuang and R. Blatt, *"Implementation of the Deutsch-Josza algorithm on an ion-trap quantum computer"*, Nature **421**, 48(2003).

[16] M.A. Nielsen anf I.L. Chuang, *"Quantum computation and quantum information"*, Cambridge University Press, ISBN: 0521635039.

[17] G. Tatara and N. Garcia, *"Quantum Toys for Quantum Computing: Persistent Currents Controlled by the Spin Josephson Effect"*, Phys. Rev. Lett. **91**, 076806 (2003).

Chapter 2

The theory of persistent currents

2.1 Basic electrodynamics

The Maxwell equations are

$$\begin{aligned} \vec{\nabla}\cdot\vec{E} &= \rho, & \vec{\nabla}\times\vec{E} + \frac{1}{c}\frac{\partial\vec{B}}{\partial t} &= 0, \\ \vec{\nabla}\cdot\vec{B} &= 0, & \vec{\nabla}\times\vec{B} - \frac{1}{c}\frac{\partial\vec{E}}{\partial t} &= \frac{\vec{j}}{c}, \end{aligned} \tag{2.1}$$

where ρ is the charge density and $\vec{j}$ the current density. The equation of motion for a charge q moving in an electromagnetic field is

$$\frac{dp}{dt} = q(\vec{E} + \vec{v}\times\vec{B}), \tag{2.2}$$

where $\vec{v}$ is the velocity of the charge. The electric field $\vec{E}$ and the magnetic field $\vec{B}$ can be defined in terms of a scalar potential ϕ and a vector potential $\vec{A}$

$$\vec{E} = -\vec{\nabla}\phi - \frac{\partial\vec{A}}{\partial t}, \qquad \vec{B} = \vec{\nabla}\times\vec{A}. \tag{2.3}$$

The potentials $\vec{A}$ and ϕ are gauge invariant, thus a transformation

$$\phi \to \phi' = \phi - \frac{df}{dt}, \qquad \vec{A} \to \vec{A}' = \vec{A} - \vec{\nabla}f, \tag{2.4}$$

for an arbitrary function $f(\vec{x}, t)$ leaves the electromagnetic fields invariant. A particularly useful gauge transformation is the Lorentz gauge

$$\frac{\partial\phi}{\partial t} + \vec{\nabla}\cdot\vec{A} = 0. \tag{2.5}$$

Using this gauge transformation allows us to rewrite the Maxwell equations to

$$\begin{aligned} \frac{1}{c^2}\frac{\partial^2}{\partial t^2}\phi - \nabla^2\phi &= \rho \\ \frac{1}{c^2}\frac{\partial^2}{\partial t^2}\vec{A} - \nabla^2\vec{A} &= \vec{j}. \end{aligned} \tag{2.6}$$

2.2 The Aharonov-Bohm effect

Aharonov and Bohm[1] proposed the following experiment, shown graphically in Fig. 2.1. A beam of electrons approaches a solenoid of radius R and is split in two parts. The solenoid extends perpendicular to the plane of the paper. The solenoid is assumed to be long, in this case there is an uniform magnetic field inside the solenoid but outside the field is zero. The magnetic flux Φ through the solenoid is defined as

$$\Phi = \int \vec{B} \cdot d\vec{S} = \oint \vec{A} \cdot d\vec{x} = \pi R^2 B. \tag{2.7}$$

The vector potential outside the solenoid is non-zero, in spherical coordinates it is given by

$$\vec{A} = \frac{\Phi}{2\pi r}\hat{\varphi}, \tag{2.8}$$

where $\hat{\varphi}$ is a unit vector in the azimuthal direction.

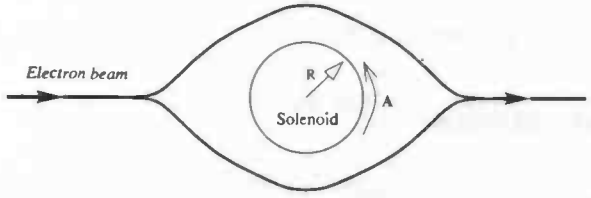

Figure 2.1: *The Aharanov-Bohm effect, a beam of electrons splits around an solenoid and recombines after passing the solenoid*

In the experiment one half of the beam will pass the solenoid in the same direction as the vector potential $\vec{A}$ and the other half will pass it in the opposing direction. Now the question is, how large is the phase shift picked up by either one of the two beams. Let ψ' be the wave function for the case $\vec{A} = 0$, the presence of a finite $\vec{A}$ changes ψ' such that it adds a phase factor g

$$\psi = e^{ig}\psi'. \tag{2.9}$$

The phase factor g is given by

$$g(\vec{r}) \equiv \frac{e}{\hbar}\int_0^{\vec{r}} \vec{A}(\vec{r'}) \cdot d\vec{r'}, \tag{2.10}$$

thus the total phase factor is

$$g = \frac{e\Phi}{2\pi\hbar c}\int \left(\frac{\hat{\varphi}}{r}\right) \cdot (r\hat{\varphi}d\varphi) = \pm\frac{e\Phi}{2\hbar c}, \tag{2.11}$$

where the plus sign corresponds to the beam which is along $\vec{A}$ and the minus sign corresponds to the beam moving in the opposite direction as $\vec{A}$. This leads to a phase difference

$$\Delta = \frac{e\Phi}{\hbar c} = \frac{2\pi\Phi}{\Phi_0}, \tag{2.12}$$

where $\Phi_0 = hc/e$ is the flux quantum.

2.3 Origin of persistent currents

When a one dimensional metallic ring is placed in a static magnetic field a current will flow[2, 3]. This current will remain present even if the magnetic field is switched off. This can be understood by noting that an electron traversing such a ring will see a periodic potential,

$$V(x + L) = V(x), \tag{2.13}$$

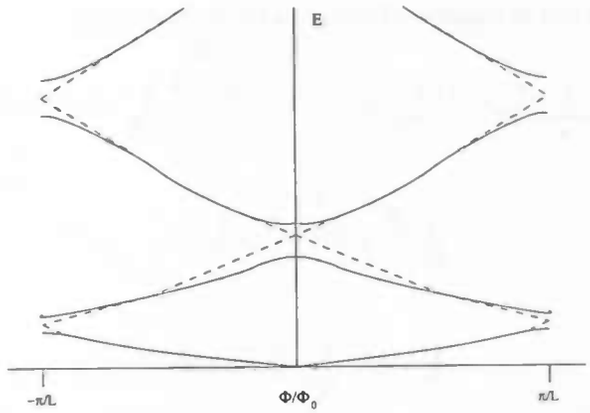

Figure 2.2: *Bandstructure of an electron in a periodic potential (solid lines), the dashed lines give the free electron case.*

where L is the length of the ring. The solution to the Schrödinger equation for such a potential is according to Bloch's theorem of the form

$$\psi(x + L) = e^{ikL}\psi(x), \tag{2.14}$$

where k is a constant. To determine k we need to know the magnitude of the phase shift an electron obtains after making a full cycle around the ring. This is determined from the Aharanov-Bohm effect discussed in the proceeding section , thus $k = \frac{2\pi\Phi}{L\Phi_0}$, which leads to the following boundary condition

$$\psi(x + L) = e^{i2\pi\Phi/\Phi_0}\psi(x). \tag{2.15}$$

The electron states are periodic in Φ with period Φ_0, the actual shape of the band structure is determined by the potential variation along the ring, see figure 2.2. When the magnetic field is not present the situation corresponds to $k = 0$. When the magnetic field is introduced the value of k will change according to

$$\frac{dk}{dt} = \frac{-eE}{\hbar}, \tag{2.16}$$

giving rise to a current. The size of the current for an electron of energy level E_n is

$$I_n = -\frac{ev_n}{L}, \qquad v_n = \frac{1}{\hbar}\frac{\partial E_n}{\partial k}, \tag{2.17}$$

using the relation $k = \frac{2\pi\Phi}{L\Phi_0}$ we can can rewrite this as

$$I_n = -c\frac{\partial E_n}{\partial \Phi}. \tag{2.18}$$

To say more about the current we need a Hamiltonian. A widely used model is the tight-binding model

$$H = -V\sum_{i=1}^{N}\sum_{\sigma}(c^{\dagger}_{i,\sigma}c_{i+1,\sigma}e^{2i\pi\Phi/N\Phi_0} + e^{-2i\pi\Phi/N\Phi_0}c^{\dagger}_{i+1,\sigma}c_{i,\sigma}) + \sum_{i=1}^{N} W_i n_i, \tag{2.19}$$

where N is the number of lattice sites, V is the hopping term, n_i is the counting operator and W_i is the on site energy. When $W_i = 0$ for all i, then the energy levels and the current can be determined analytically[3] by diagonalizing the Hamiltonian. This can be achieved most easily by going to Fourier space. We substitute

$$c_{j,\sigma} = \frac{1}{\sqrt{N}}\sum_{k} c_{k,\sigma}e^{ikj}, \tag{2.20}$$

with $k = 2\pi m/N$. Inserting this in equation (2.19) gives for the first term

$$\frac{1}{N}\sum_j c^\dagger_{j,\sigma}c_{j+1,\sigma} = \frac{1}{N}\sum_j\sum_k c^\dagger_{k,\sigma}e^{-ikj}\sum_{k'} c^\dagger_{k',\sigma}e^{-ik'(j+1)} = \frac{1}{N}\sum_{k,k'} c^\dagger_{k,\sigma}c_{k',\sigma}e^{ik'}\sum_{j=1}^{N} e^{-ij(k-k')}. \quad (2.21)$$

As

$$\frac{1}{N}\sum_{j=1}^{N} e^{-ij(k-k')} = \delta_{k,k'}, \quad (2.22)$$

we finally get

$$\sum_j c^\dagger_{j,\sigma}c \sum_k c^\dagger_{k,\sigma}c_{k,\sigma}e^{ik}. \quad (2.23)$$

Using this we can rewrite the Hamiltonian (2.19) as

$$\begin{aligned} H &= -V\sum_k\sum_\sigma (c^\dagger_{k,\sigma}c_{k,\sigma}e^{ik}e^{2i\pi\phi/\phi_0 N} + e^{-2\pi\phi/\phi_0}e^{-ik}c^\dagger_{k,\sigma}c_{k,\sigma}), \\ &= -V\sum_k\sum_\sigma (c^\dagger_{k,\sigma}c_{k,\sigma}(e^{i(k+2\pi\phi/\phi_0 N)} + e^{-i(k+2\pi\phi/\phi_0 N)}), \\ &= -2V\sum_k\sum_\sigma (\cos(k + 2\pi\phi/\phi_0 N)c^\dagger_{k,\sigma}c_{k,\sigma}. \end{aligned} \quad (2.24)$$

This matrix is diagonal in k. Thus all eigenvalues are (substituting $k = 2\pi m/N$)

$$E_n = -2V\cos(\frac{2\pi}{N}[n + \Phi/\Phi_0]), \quad (2.25)$$

and the current is given by

$$I_n = -\frac{2eV}{N\hbar}\sin(\frac{2\pi}{N}[n + \Phi/\Phi_0]). \quad (2.26)$$

To calculate the total current for a system with m electrons we have to sum over the m eigenstates that are lowest in energy. The crucial step now is to determine over which states we have to sum. The most obvious choice is to find a region for Φ/Φ_0 so that we can take $n = 0, \pm1, \pm2, \ldots$ as the first m eigenstates. There is a difference between the case when we have an odd number of electrons and when we have an even number of electrons. In the case of an even number of electrons the states

$$\frac{N_e}{2} \le n < \frac{N_e}{2} - 1, \quad (2.27)$$

are lowest in energy for $0 \le \Phi/\Phi_0 < 1$. When we have an odd number of electrons the states,

$$-\frac{N_e - 1}{2} \le n < \frac{N_e - 1}{2}, \quad (2.28)$$

are lowest in energy when $-\frac{1}{2} \le \Phi/\Phi_0 < \frac{1}{2}$. Summing over the appropriate eigenstates will give the total current [3]

$$I = \begin{cases} -I_0\frac{\sin(2\pi\phi/N\phi_0)}{\sin(\pi/N)} & N_e \text{ odd} \quad -0.5 \le \frac{\phi}{\phi_0} < 0.5 \\ -I_0\frac{\sin(2\pi\phi/N\phi_0 - \pi/N)}{\sin(\pi/N)} & N_e \text{ even} \quad 0 \le \frac{\phi}{\phi_0} < 1 \end{cases}, \quad (2.29)$$

with $I_0 = \frac{2eV}{N\hbar}\sin(\frac{\pi N_e}{N}) = \frac{ev_F}{L}$.

In Figs. 2.3(a)-(b) we plot one period of the total current (2.29) for two different N. For small N the shape of the total current is still slightly curved but when N is increased, very quickly a seesaw like shape appears.

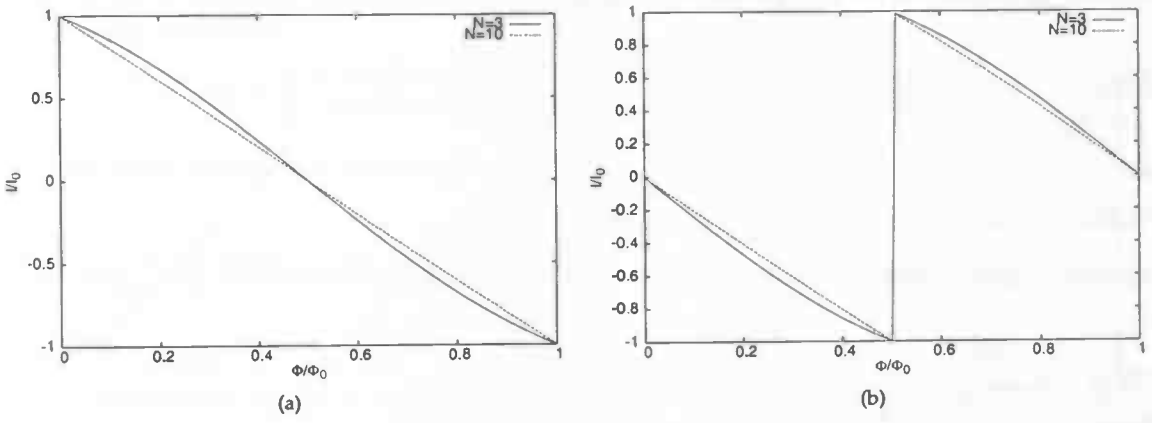

Figure 2.3: *The current* I *for (a) even* N_e *and (b) odd* N_e.

Now we are going to consider the case when electron spin is taken into account. Each state in (2.25) can now be occupied by two electrons. There is again a distinction between the case of an even number of electrons and when we have an odd number of electrons

$$I_{spin} = \begin{cases} 2I_{ns}(\frac{N_e}{2}) & N_e \text{ is even} \\ I_{ns}(\frac{N_e+1}{2}) + I_{ns}(\frac{N_e-1}{2}) & N_e \text{ is odd,} \end{cases} \tag{2.30}$$

where $I_{ns}(z)$ is the total current in the case of z spinless electrons determined by equation (2.29). Thus we can understand the current in the case with electron spin taken into account in terms of the spinless case. For example when $N_e = 5$ we find $I_{spin} = I_{ns}(3) + I_{ns}(2)$

We are now going to work out the case when N_e is odd. Here we have to sum over an even I_{ns} and an odd I_{ns} as defined in equation (2.29). However when doing this summation there is an complication, the domains of Φ/Φ_0 do not overlap completely. We need to define[1] I_{ns} for odd N_e^{ns} on the region $\frac{1}{2} \leq \Phi/\Phi_0 < 1$. This is easily done by noting that in the region $\frac{1}{2} \leq \Phi/\Phi_0 < 1$ the lowest energy states are centered around $n = -1$. Thus we need to sum over the states

$$-\frac{N_e^{ns}+1}{2} \leq n \leq \frac{N_e^{ns}-3}{2}, \tag{2.31}$$

doing this summation yields

$$I_{ns} = -I_0 \frac{\sin(2\pi(\phi/\phi_0 - 1)/N)}{\sin(\pi/N)} \quad N_e^{ns} \text{ is odd} \quad 0.5 \leq \frac{\Phi}{\Phi_0} < 1.5\,. \tag{2.32}$$

To compute the total current we need to consider two different cases

1. $\frac{N+1}{2}$ is even, then the total current becomes (from (2.30)),

$$I_{spin} = -\frac{2eV}{N\hbar} \begin{cases} \sin(\pi\frac{N_e+1}{2N})\frac{\sin(2\pi\phi/N\phi_0 - \pi/N)}{\sin(\pi/N)} + \sin(\pi\frac{N_e-1}{2N})\frac{\sin(2\pi\phi/N\phi_0)}{\sin(\pi/N)} & 0 \leq \Phi/\Phi_0 < \frac{1}{2} \\ \sin(\pi\frac{N_e+1}{2N})\frac{\sin(2\pi\phi/N\phi_0 - \pi/N)}{\sin(\pi/N)} + \sin(\pi\frac{N_e-1}{2N})\frac{\sin(2\pi(\phi/\phi_0-1)/N)}{\sin(\pi/N)} & \frac{1}{2} \leq \Phi/\Phi_0 < 1 \end{cases} \tag{2.33}$$

2. $\frac{N+1}{2}$ is odd, then the total current becomes,

$$I_{spin} = -\frac{2eV}{N\hbar} \begin{cases} \sin(\pi\frac{N_e+1}{2N})\frac{\sin(2\pi\phi/N\phi_0)}{\sin(\pi/N)} + \sin(\pi\frac{N_e-1}{2N})\frac{\sin(2\pi\phi/N\phi_0 - \pi/N)}{\sin(\pi/N)} & 0 \leq \Phi/\Phi_0 < \frac{1}{2} \\ \sin(\pi\frac{N_e+1}{2N})\frac{\sin(2\pi(\phi/\phi_0-1)/N)}{\sin(\pi/N)} + \sin(\pi\frac{N_e-1}{2N})\frac{\sin(2\pi\phi/N\phi_0 - \pi/N)}{\sin(\pi/N)} & \frac{1}{2} \leq \Phi/\Phi_0 < 1 \end{cases} \tag{2.34}$$

[1] N_e^{ns} is the number of electrons in I_{ns}.

In Figs. 2.4(a)-(b) we plot the total current in a ring of 30 sites for $N_e = 3$ and $N_e = 5$.

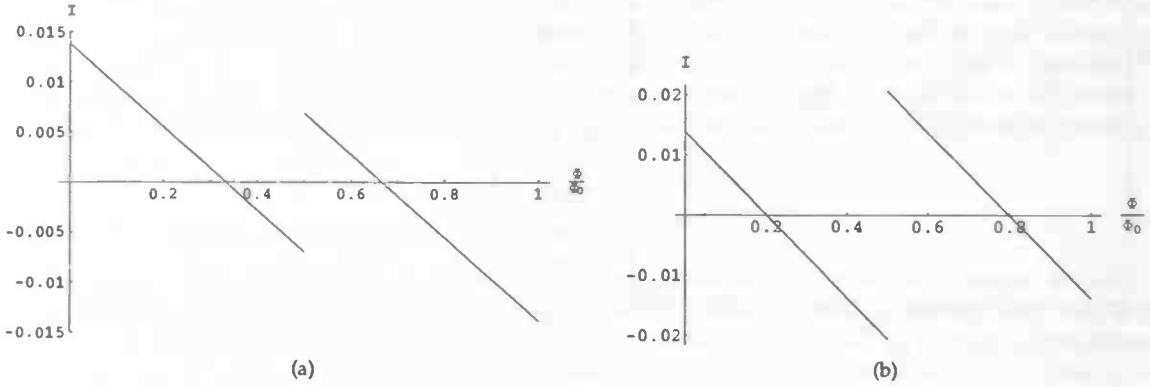

Figure 2.4: *Total current for a ring of* $N = 30$ *sites with in (a)* $N_e = 3$ *electrons and in (b)* $N_e = 5$ *electrons.*

It is quite unfortunate that equations (2.33) and (2.34) cannot be simplified. However when N is large we can make the following approximation. We replace the factors $N_e + 1/2N$ and $(N_e - 1)/2N$ in equations (2.33) and (2.34) by $N_e/2N$. In figures 2.4(a)-(b) the current in the interval $1/2 \leq \Phi/\Phi_0 < 1$ is the same as that in the interval $0 \leq \Phi/\Phi_0 < 1/2$ except that it is shifted in the "y" direction. When N increases this shift in the "y" direction will become less and less and it is this shift that we ignore in our approximation. This leads to a $\Phi/2\Phi_0$ periodicy, with a total current given by

$$I_{spin} = -I_0' \frac{\sin(\pi(2\phi/\phi_0 - 1/2)/N)}{\sin(\pi/2N)} \quad 0 \leq \frac{\phi}{\phi_0} < \frac{1}{2} \quad N_e \text{ is odd} \tag{2.35}$$

with $I_0' = \frac{2eV}{N\hbar} \sin(\frac{\pi N_e}{2N})$. To show the validity, we plot for a ring of 30 sites the case with $N_e = 17$ both from equation (2.34) and equation (2.35). Clearly the approximation here is very good.

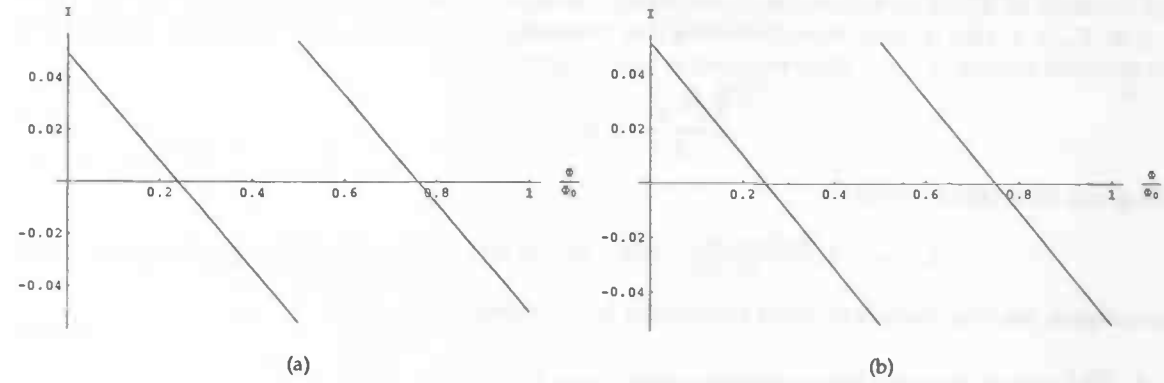

Figure 2.5: *Comparison between current computed with equation* (2.34) *and* (2.35) *for* $N = 30$ *and* $N_e = 17$, *where (a) is calculated from equation* (2.34) *and (b) is calculated from equation* (2.35)

2.4 The effect of disorder

When disorder is present we cannot derive a general analytical expression for the current. The size of the persistent current will dependent on the nature of the disorder. Consider a random potential with strength W, so that $-W/2 \leq W_i \leq W/2$. We can analyze this situation with a transfer-matrix approach, following Cheung, et al.[3].

We can assign to each site j a transfer matrix T_j, that connects site j to sites $j-1$ and site $j+1$. We can write the wave function as

$$\psi(x) = \begin{cases} Ae^{ik(x-(j-1/2)a)} + Be^{-ik(x-(j-1/2)a)} & x = (j-1)a, ja \\ Ce^{ik(x-(j+1/2)a)} + De^{-ik(x-(j+1/2)a)} & x = ja, (j+1)a \end{cases}, \tag{2.36}$$

with a the lattice spacing. The energy is given by

$$E(k) = -2V\cos(ka). \tag{2.37}$$

We now impose the continuity condition and that the wave function obeys the tight-binding Schrödinger equation

$$\begin{pmatrix} e^{ika/2} & e^{-ika/2} \\ -Ve^{-ika/2} + (W-E)e^{ika/2} & -Ve^{ika/2} + (W-E)e^{-ika/2} \end{pmatrix} \begin{pmatrix} A \\ B \end{pmatrix} = \begin{pmatrix} e^{-ika/2} & e^{ika/2} \\ Ve^{ika/2} & Ve^{-ika/2} \end{pmatrix} \begin{pmatrix} C \\ D \end{pmatrix}. \tag{2.38}$$

Rewriting this gives T_j

$$\begin{pmatrix} C \\ D \end{pmatrix} = \begin{pmatrix} e^{ika}/t_j^* & r_j/t_j \\ r_j^*/t_j^* & e^{-ika}/t_j \end{pmatrix} \begin{pmatrix} A \\ B \end{pmatrix} = T_j \begin{pmatrix} A \\ B \end{pmatrix}, \tag{2.39}$$

where the reflection coefficient t_j and the transmission coefficient r_j are given by,

$$t_j = \frac{2iV\sin(ka)}{2iV\sin(ka) - W_i}, \qquad r_j = t_j - 1 = \frac{W_i}{2iV\sin(ka) - W_i}. \tag{2.40}$$

Starting with some initial coefficients A and B at site j we can use this transfer matrix to calculate the wave function at sites $j+1, j+2, \ldots$. After applying this procedure N times (for a ring with N sites) we are back at site j, the transfer matrix we have obtained by this procedure is called the total transfer matrix and is defined by,

$$T = \prod_{j=0}^{j=N} T_j = \begin{pmatrix} 1/t^* & r/t \\ r^*/t^* & 1/t \end{pmatrix}, \tag{2.41}$$

where r and t are the total reflection and transfer coefficients. Of course boundary condition (2.15) must hold. Thus we have

$$T \begin{pmatrix} A \\ B \end{pmatrix} = e^{i2\pi\phi/\phi_0} \begin{pmatrix} A \\ B \end{pmatrix}. \tag{2.42}$$

For this condition to hold $e^{i2\pi\phi/\phi_0}$ must be a eigenvalue of T. Thus the relation $\det(T - e^{i2\pi\phi/\phi_0}) = 0$ holds. Writing out this relation gives

$$\cos(2\pi\phi/\phi_0) = \mathrm{Re}(1/t) \equiv f(E), \tag{2.43}$$

where we have used the relation $|r|^2 + |t|^2 = 1$. The matching condition $f(E)$ determines the allowed values for k and thus also determines the eigenenergies. When we evaluate $f(E)$ at energy level E_n we find that the current I_n is just

$$I_n = -c\frac{\partial E}{\partial \phi} = -c\frac{\partial f}{\partial \phi}\frac{\partial E}{\partial f} = \frac{e}{\hbar}\frac{\sin(2\pi\phi/\phi_0)}{\frac{\partial}{\partial E}\mathrm{Re}(1/t)}. \tag{2.44}$$

This is our central result. We can now calculate the persistent current for a given potential distribution by just by simply multiplying all the transfer matrices T_j and reading of the resulting transmission coefficient t.

2.4.1 Localization

In a randomly disordered system, a phenomenon called localization may occur (for a review see Ref. [4] or Ref. [5]). The phenomenon was discovered by Anderson in 1957[6]. Loosely speaking a localized state

is a state that is confined to a certain region in space. Consider for example an infinite rod containing a random impurity potential along the rod. At time $t = 0$ we put a wave packet at location $x = 0$ on the rod. As time goes by the wave packet diffuses. In the absence of a potential the wave packet would at $t = \infty$ have diffused to $x = \pm\infty$. The presence of the random potential leads to back scattering of the wave packet. At $t = \infty$ the wave packet will not have diffused to infinity but will be confined to a certain region of space. The width of this region depends on the strength of the disorder. Of course the wave packet will not be strictly confined to a region. Instead the wave function will decay exponentially along the rod,

$$|\Psi(r)| \propto e^{-|r-r_0|/\xi}, \tag{2.45}$$

where ξ is the localization length.

In the presence of a random disorder potential, 1- and 2-dimensional systems will always be localized. If the strength of the potential is weak, the localization length can become extremely large and such a system will effectively behave like a delocalized system. In three dimensions the strength of the disorder will determine if a state is localized or not. If a state is localized then at temperature $T = 0$ the system will be an insulator. If it is delocalized then the system will be a conductor.

In the following we will focus on our 1-dimensional rings. The fact that it is a ring makes the system special in this context, because the localization length can be larger then the ring. We expect a negative influence of the disorder on the size of the persistent current[2] because of the localization effect. Indeed the current is highly dependent on the localization length. When the localization length is larger than the ring, he current will be hindered little by the disorder. This is what we call *weak disorder* in this context. When the localization length becomes smaller then the size of the ring, the current will be reduced dramatically. This limit is called *strong disorder*.

For the half-filled case an estimate can be made for the localization length ξ in two limits[3]

$$\begin{aligned} \xi &= \frac{105aV^2}{W^2}, && (W \ll 2\pi V) \\ \xi &= \frac{a}{\log(W/2eV)}, && (W \gg 2\pi V) \end{aligned} \tag{2.46}$$

where a is the lattice constant. Normally in a persistent current experiment we are interested in the first limit. It can be shown that the current in this limit for the half filled case is

$$I = \frac{1}{2} I_0 e^{-L/\xi}, \qquad (W \ll 2\pi V) \tag{2.47}$$

with $I_0 = ev_f/Na$.

2.5 Experimental results

Copper

There have been a number of experimental observations of persistent currents. the most famous experiment is the one by Levy et al. [9] who were the first to observe a persistent current experimentally. In the experiment 10^7 isolated copper rings were put in a slowly varying magnetic field. These rings were actually squares with a circumference of 2.2 μm. The size of the persistent current measured was $I = 3 \times 10^{-3} ev_f/L$ per ring. But surprisingly the current was periodic in Φ with period $\Phi_0/2$ instead of the expected Φ_0 periodicy.

This period halving is actually an averaging effect which is most easily shown in case of spinless electrons[3] by considering the Fourier spectrum of the current[3]. The l'th Fourier coefficient is proportional to $\cos(lk_f L)$ with $k_f = N_e\pi/L$. The Fourier coefficient as a function of N_e alternates sign for odd l but

[2] Although scattering effects can in some cases lead to an enhancement of the current.

[3] The situation is more complex when spin is included, but the periodicy is the same[8].

is positive for even l. In the ensemble of copper rings, each ring can have a different (randomly distributed) number of electrons N_e. Although because the rings are isolated from each other N_e stays constant in each ring. Because the odd Fourier coefficients alternate in sign as a function of N_e, only the even Fourier components survive the averaging. This leads to an halving of both the period and the amplitude.

Gold

The first experiment using gold rings was done by Chandrasekhar et al.[9]. They measured the magnetic response in single gold loops. Thus in contrast to the experiment of Levy we do not have to deal with averaging effects in this experiment, which means that we can compare these measurements straightforwardly against the numerical calculations of section 4.4.3. Three different loops were used, two rings of 2.4 μm and 4,0 μm diameter and the third loop was an square with dimensions 1.4 μm × 2.6 μm. They found an persistent current I of $0.3ev_f/L \leq I \leq 2.0ev_f/L$ at temperature T = 10 mK.

A second experiment using 30 gold rings was done by Jariwala et al.[8]. The rings had length $L = 8.0 \pm 0.2\,\mu m$ of thickness 60 ± 2 nm and width 120 ± 20 nm. The persistent current measured is an average over the 30 rings. Because of the small number of rings now both an Φ_0 periodic and $\Phi_0/2$ periodic component is present. The Φ_0 periodic component of the current $I_{h/e} = 4.57 \times 10^{-3} ev_f/L$ and the $\Phi_0/2$ periodic component is $I_{h/e} = -4.78 \times 10^{-3} ev_f/L$ per ring. Because of the small number of rings, the measured current is not a true ensemble average. It is therefore questionable if we can use these results to test against in our numerical results.

GaAs-AlGaAs

A third kind of experiment is using a GaAs-AlGaAs semiconductor In such a system a layer of AlGaAs (an alloy of AlAs and GaAs) is embedded between two layer of GaAs. Because AlGaAs has nearly the same lattice structure as GaAs, but with a larger band gap, a thin essentially two dimensional conduction layer occurs at the boundary between the layers. Mailly et al. [11] measured the current in a single GaAs-AlGaAs loop, consisting of a 720 nm buffer layer, a 24 nm undoped AlGaAs spacer layer, a 48 nm Si doped AlGaAs layer and a 10 nm GaAs cap layer. The ring is cooled with liquid helium. At this low temperature the electron density at the heterointerface is $\rho_{el} = 3.6 \times 10^{11}\,cm^{-2}$, the Fermi velocity $v_f = 2.6 \times 10^4$ m/s and the elastic mean free path $l = 11\,\mu m$. The internal diameter of the ring is 2 μm and the line thickness 0.7 μm. The measured current I was found to be $0.4ev_f/L \leq I \leq 1.2ev_f/L$ which is of the same order as the value expected for a disorderless system, $I = ev_f/L$.

Rabaud et al.[13] did an experiment on an ensemble of 10^5 connected rings consisting of a 1 μm buffer layer, a 15 nm undoped AlGaAs spacer layer, a 48 nm Si doped AlGaAs layer and a 5 nm GaAs cap layer. The ring is cooled to 4.2 K. At this low temperature the electron density at the heterointerface is $\rho_{el} = 5.2 \times 10^{11}\,cm^{-2}$, the Fermi velocity $v_f = 3.16 \times 10^5$ m/s and the elastic mean free path $l = 8\,\mu m$.The rings are actually squares with an internal side length of 2 μm and the line thickness is 1.0 μm. Because we are taking an ensemble average the observed current I had a periodicy of $\Phi/2$ due to the averaging effect we discussed previously in connection to Levy's experiment. The size of the current was found to be $I = (9.48 \pm 1.9) \times 10^{-2} ev_f/L$. The experiment was repeated for the case where all rings were disconnected. Surprisingly the current was found to be similar to that of the connected rings. Thus according to this experiment the difference between an ensemble of connected rings and an ensemble of disconnected rings is negligible.

2.6 Dephasing rate and persistent currents

From the above it should be clear that the present theory underestimates the persistent current by one to two orders of magnitude. There is a second unsolved problem in mesoscopic physics that might be

related to the problem of the persistent currents. The dephasing rate is theoretically expected to go to zero when the temperature approaches $T = 0$. Mohanty et al. [15] however showed experimentally that in reality the dephasing rate becomes constant at low temperatures. Kravtsov and Altshuler proposed that that these two problems might be connected[14]. Unlike what is normally assumed they proposed that a ring in a static magnetic field is not an equilibrium system. Non-equilibrium noise (of whose origin no assumptions are made) can induce an ac electrical field. It is also known that an ac electric field can induce a dc current[16]. The central result of Ref. [14] is that there is a relation between the noise induced current I and the dephasing rate τ_ϕ caused by that same noise

$$I\tau_\phi = C_\beta e, \qquad C_\beta = \begin{cases} -4/\pi, & \beta = 1, \\ 2/\pi, & \beta = 4, \end{cases} \tag{2.48}$$

where the constant C_β depends on the Dyson symmetry class. $\beta = 1$ for the pure potential disorder and $\beta = 4$ when spin-orbit scattering is present. Kravtsov and Altshuler compared Equation (2.48) to experiment in their paper [14], the results are listed in table 2.1. The agreement between equation (2.48) and experiment is remarkably good, however it is clear that equation (2.48) is also unable to make an accurate prediction of the persistent current.

Experiment	Observed current	Current according to eq. (2.48)
10^5 GaAs-AlGaAs rings [12]	1.50 nA	< 1.20 nA
10^7 copper rings [9]	0.30 nA	< 0.90 nA
30 gold rings [8]	0.06 nA	0.03 nA

Table 2.1: *Comparison between equation (2.48) and experiment taken from [14].*

Bibliography

[1] Y. Aharanov and D. Bohm, *"Significance of Electromagnetic Potentials in the Quantum Theory"*, Phys. Rev. **115**, 485 (1959).

[2] M. Buttiker, Y. Imry and R. Landauer, *"Josephson behavior in small normal one-dimensional rings"*, Phys. Lett. **96A**, 365 (1983).

[3] H. Cheung, Y. Gefen, E. K. Riedel and W. Shih, *"Persistent currents in small one-dimensional metal rings"*, Phys. Rev. B **37**, 6050 (1988)

[4] B. Kramer and A. MacKinnon, *"Localization: theory and experiment"*, Rep. Prog. Phys. **56**, 1469 (1993).

[5] P.A. Lee and T.V. Ramakrishnan, *"Disordered Electronic Systems"*, Rev. Mod. Phys. **57**, 287 (1985).

[6] P.W. Anderson, *"Absence of Diffusion in Certain Random Lattices"*, Phys. Rev. **1958**, 1492 (1958).

[7] L.P. Levy, G. Dolan, J. Dunsmuir and H. Bouchiat, *"Magnetization of Mesoscopic Copper Rings : Evidence for Persistent Currents."*, Phys. Rev. Lett. **64** 2074 (1990)

[8] D. Loss and P. Goldbart, *"Period and amplitude halving in mesoscopic rings with spin"*, Phys. Rev. B **43** 13762 (1991)

[9] V. Chandrasekhar, R. A. Webb, M. J. Brady, M. B. Ketchen, W. J. Gallagher, and A. Kleinsasser,*"Magnetic response of a single, isolated gold loop"*, Phys. Rev. Lett. **67** 3578 (1991)

[10] E.M.Q. Jariwala, P. Mohanty, M.B. Ketchen and R.A. Webb, *"Diamagnetic Persistent Current in Diffusive Normal-Metal Rings"*, Phys. Rev. Lett. **86** 1594 (2001)

[11] D. Mailly, C. Chapelier and A. Benoit, *"Experimental observation of Persistent Currents in a GaAs-AlGaAs Single Loop"*, Phys. Rev. Lett. **70**, 2020(1993)

[12] B. Reulet1, M. Ramin, H. Bouchiat and D. Mailly, *"Dynamic Response of Isolated Aharonov-Bohm Rings Coupled to an Electromagnetic Resonator"*, Phys. Rev. Lett. **75**, 124 (1995)

[13] W. Rabaud, L. Saminadayar, D. Mailly, K. Hasselbach, A. Benoit and B. Etienne, *"Persistent Currents in Mesoscopic Connected Rings"*, Phys. Rev. Lett. **86**, 3124 (2001).

[14] V.E. Kravtsov and B.L. Altshuler, *"Relationship between the Noise-Induced Persistent Current and the Dephasing Rate"*, Phys. Rev. Lett. **84**, 3394(2000).

[15] P. Mohanty, E.M.Q. Jariwala and R.A. Webb,*"Intrinsic Decoherance in Mesoscopic Systems"*, Phys. Rev. Lett. **78**, 3366(1997)

[16] V.E. Kravtsov and V.I. Yudson, *"Direct current in mesoscopic rings induced by high-frequency electromagnetic field"*, Phys. Rev. Lett. **70**, 210(1993).

Chapter 3

Numerical methods

3.1 Introduction

3.1.1 Partial differential equations

To do a simulation of a quantum mechanical system basically means solving the Schrödinger equation, which is a second order partial differential equation. In general a linear second order partial differential equation(PDE) is of the form,

$$A\frac{\partial^2 u}{\partial x^2} + 2B\frac{\partial^2 u}{\partial x \partial y} + C\frac{\partial^2 u}{\partial y^2} + D\frac{\partial u}{\partial x} + E\frac{\partial u}{\partial y} + Fu + g = 0. \tag{3.1}$$

We can classify a PDE according to the determinant of the matrix,

$$Z = \begin{pmatrix} A & B \\ B & C \end{pmatrix}, \tag{3.2}$$

- If det(Z)>0 then the PDE is elliptic, an example of an elliptic PDE is the Poison equation,

$$\nabla^2 u(x,y) = f(x,y). \tag{3.3}$$

- If det(Z)<0 then the PDE is hyperbolic, an example of a PDE of this type is the wave equation,

$$\nabla^2 u(x,t) = \frac{\partial^2 u(x,t)}{\partial t^2}. \tag{3.4}$$

- If det(Z)=0 then the PDE is parabolic, two examples of parabolic PDE are the heat equation,

$$\nabla^2 u(x,t) = \frac{\partial u(x,t)}{\partial t}, \tag{3.5}$$

and the Schrödinger equation,

$$-\frac{\hbar^2}{2m}\nabla^2\psi(x,t) + V(x)\psi(x,t) = i\hbar\frac{\partial\psi(x,t)}{\partial t}. \tag{3.6}$$

3.1.2 Stability

A loose definition of stability would be that a numerical method is stable when a small change in the input parameters yields a small change in the results of the method.

The methods we are interested in are so called iteration methods. In such a method we start with a vector $w^{(0)}$, which is given as an initial condition. Then we repeatedly apply a $n \times n$ matrix A characterizing the method to the result vector $\vec{w}$. Thus at the n'th step of the method we have,

$$\vec{w}^{(n)} = A\vec{w}^{(n-1)}. \tag{3.7}$$

To actually prove when such a method is stable, we need some results from matrix theory. We will now give the theory needed to prove stability for iteration methods.

We will start with the norm of a matrix. In the case of the vector there exist an intuitive norm, namely the length of that vector. For a matrix the concept of a norm is much less intuitive, we define the matrix norm formally below.

Definition 1 *A matrix norm on the set of all $n \times n$ matrices is a real valued function $\|\cdot\|$, satisfying for all $n \times n$ matrices A and B and all real numbers α,*

- $\|A\| > 0$,
- $\|A\| = 0$ if and only if $A = 0$,
- $\|\alpha A\| = |\alpha|\|A\|$,
- $\|A + B\| \leq \|A\| + \|B\|$,
- $\|AB\| \leq \|A\|\|B\|$.

In the following we will frequently use the notion of a natural matrix norm.

Definition 2 *If $\|\cdot\|$ is a vector norm on $\mathbb{R}^n$, $\vec{x} \in \mathbb{R}^n$ and A is a $n \times n$ matrix then,*

$$\|A\| = \max \|A\vec{x}\|, \qquad \text{with } \|\vec{x}\| = 1,$$

is the natural matrix norm associated with the vector norm.

An important quantity of a matrix A is that of the magnitude of its largest eigenvalue, which is called the spectral radius.

Definition 3 *The spectral radius $\rho(A)$ of a matrix A is defined by, $\rho(A) = \max|\lambda|$, where λ is an eigenvalue of A.*

A very useful result is that we can link the spectral radius of a matrix A to its norm.

Theorem 3 *For any $n \times n$ matrix A and natural matrix norm $\|\cdot\|$ we have, $\rho(A) \leq \|A\|$*

Proof : For $\vec{x} \in \mathbb{R}^n$ with $\|\vec{x}\| = 1$ and λ an eigenvalue of A,

$$\|\lambda\| = \|\lambda\|\|\vec{x}\| = \|\lambda\vec{x}\| = \|A\vec{x}\| \leq \|A\|\|x\| = \|A\|,$$

thus $\rho(A) \leq \|A\|$. □

We can for all matrices A define a natural matrix norm $\|\cdot\|$ in such a way that $\|A\|$ comes arbitrarily close to $\rho(A)$.

Theorem 4 *For each $n \times n$ matrix A and each arbitrary $\epsilon > 0$ there exists a natural norm $\|\cdot\|$ such that,*

$$\rho(A) \leq \|A\| \leq \rho(A) + \epsilon$$

For the proof we refer the reader to Ref. [1].

A very important matrix property for numerical methods is that of convergence. We will later find that convergent matrices necessarily represent a stable method.

Definition 4 *A $n \times n$ matrix A is convergent when $\lim_{n\to\infty}(A^n)_{i,j} = 0$, for all matrix elements i, j.*

Thus for a convergent matrix A, we have for any natural norm $\|A\| < 1$. We can use this fact together with the theorems defined up to this point to give a very useful condition for convergence.

Theorem 5 *A $n \times n$ matrix A is convergent if and only if* $\rho(A) < 1$

Proof : From theorem 3 we know,

$$\|A^n\| \geq \rho(A^n) = \rho^n(A)$$

From theorem 4 we know that we can find a natural matrix norm $\|\cdot\|$ and scalar ϵ such that,

$$\|A\| \leq \underbrace{\rho(A) + \epsilon}_{\theta} < 1.$$

But, $\|A^n\| \leq \|A\|^n \leq \theta^n$, meaning that,

$$\lim_{n\to\infty} (\|A\|^n) = 0,$$

which is just the definition of convergence. □

Now finally we have developed all the mathematics necessary to prove when an iteration method is convergent. Suppose that our iteration method starts with an error $e^{(0)}$ in the initial data $w^{(0)}$. As we noted at the beginning of this section, the method can only be stable when this error does not grow after each step. Meaning that for the matrix A characterizing the method we have the following condition for stability,

$$A^n e^{(0)} \leq e^{(0)}.$$

Thus according to theorem 5 if A is convergent then it is necessarily stable. But what about the case where A is unitary, thus when $\|A\| = 1$? We can easily prove that in this case $\rho(A) = 1$.

Theorem 6 *If the $n \times n$ matrix A is unitary, then* $\rho(A) = 1$.

Proof : For an unitary matrix A, the equality $A = A^{-1}$ holds. But if $\lambda = 1$ is an eigenvalue of A, then λ^{-1} is an eigenvalue of A^{-1}. This can only be the case if $|\lambda| = |\lambda^{-1}| = 1$. □

Now to summarize our results, an iteration method is stable if and only if $\rho(A) \leq 1$.

3.2 The Cranck-Nicholson method

We will now derive the Cranck-Nicholson method, this is a method for parabolic PDE's (like the Schrödinger equation). We will start by discretizing the parabolic PDE

$$\frac{\partial u}{\partial t} = \alpha^2 \frac{\partial^2 u}{\partial x^2}, \tag{3.8}$$

for this we use the difference methods

$$\frac{\partial u(x_i, t_j)}{\partial t} = \frac{u(x_i, t_j) - u(x_i, t_j - k)}{k} + O(k^2), \tag{3.9}$$

$$\frac{\partial^2 u(x_i, t_j)}{\partial x^2} = \frac{u(x_i + h, t_j) - 2u(x_i, t_j) + u(x_i - h, t_j)}{\delta^2} + O(\delta^3). \tag{3.10}$$

Using the notation $w_{i,j} = u(x_i, t_j)$, we can rewrite the PDE as

$$\frac{w_{i,j} - w_{i,j-1}}{k} + \alpha^2 \frac{w_{i+1,j} - 2w_{i,j} + w_{i-1,j}}{\delta^2} = 0. \tag{3.11}$$

Given an initial state $w(i,0)$, we can write each $w_{i,j}$ in terms of $w_{i,j-1}$ and thus solve the PDE using the iteration $Aw^{(n)} = w^{(n-1)}$ with

$$A = \begin{pmatrix} 1+2\gamma & -\gamma & 0 & \dots & 0 \\ -\gamma & \ddots & \ddots & \ddots & \vdots \\ 0 & \ddots & \ddots & \ddots & 0 \\ \vdots & \ddots & \ddots & \ddots & -\gamma \\ 0 & \dots & 0 & -\gamma & 1+2\gamma \end{pmatrix}, \tag{3.12}$$

where $\gamma = \frac{\alpha^2 k}{\delta^2}$. This method is called the backward-difference method and it is of order $O(k+\delta^2)$. The eigenvalues of A are

$$\lambda_j = 1 + 4\gamma \left[\sin\left(\frac{j\pi}{2(N+1)}\right)\right]^2, \qquad \text{for} j = 1,2,\dots,N \tag{3.13}$$

As we want to calculate w^n from w^{n-1}, the method is stable if $\rho(A^{-1}) \leq 1$. As $\lambda_j \geq 1$ this is the case for any γ. Because the method is stable for all parameters γ, we call this method unconditionally stable. Because this method only has linear convergence in time, it is desirable to improve this method so that it is also quadratically convergent in time. This can be done by using the forward difference expression

$$\frac{w_{i,j+1} - w_{i,j}}{k} - \alpha^2 \frac{\hbar^2}{2m} \frac{w_{i+1,j} - 2w_{i,j} + w_{i-1,j}}{\delta^2} = 0, \tag{3.14}$$

we could derive from this expression a forward-difference method in the same way we did for the backward-difference method. But if we average the *forward* difference method at time step j with the *backward* difference method at time step j + 1 then we get the expression

$$\frac{w_{i,j+1} - w_{i,j}}{k} + \frac{\alpha^2}{2}\left[\frac{w_{i+1,j} - 2w_{i,j} + w_{i-1,j}}{\delta^2} + \frac{w_{i+1,j+1} - 2w_{i,j+1} + w_{i-1,j+1}}{\delta^2}\right] = 0, \tag{3.15}$$

leading to the iteration $Aw^{(n+1)} = Bw^{(n)}$ with

$$A = \begin{pmatrix} 1+\gamma & -\gamma/2 & 0 & \dots & 0 \\ -\gamma/2 & \ddots & \ddots & \ddots & \vdots \\ 0 & \ddots & \ddots & \ddots & 0 \\ \vdots & \ddots & \ddots & \ddots & -\gamma/2 \\ 0 & \dots & 0 & -\gamma/2 & 1+\gamma \end{pmatrix}, B = \begin{pmatrix} 1-\gamma & \gamma/2 & 0 & \dots & 0 \\ \gamma/2 & \ddots & \ddots & \ddots & \vdots \\ 0 & \ddots & \ddots & \ddots & 0 \\ \vdots & \ddots & \ddots & \ddots & \gamma/2 \\ 0 & \dots & 0 & \gamma/2 & 1-\gamma \end{pmatrix}, \tag{3.16}$$

where again $\gamma = \frac{\alpha^2 k}{\delta^2}$. This method is called the Crank-Nicholson method which is of order $O(k^2 + \delta^2)$[1]. The Crank-Nicholson method is an unitary method [3] and is therefore unconditionally stable. Unfortunately, to compute $w^{(n+1)} = A^{-1}Bw^{(n)}$, we need to invert the matrix A, making this method inefficient for large matrices.

3.3 The Suzuki-Trotter method

An alternative approach is to discretize the solution of the Schrödinger equation, in general we can write the Schrödinger equation in the form,

$$i\hbar\frac{\partial}{\partial t}\psi = H\psi, \tag{3.17}$$

[1]For more details we refer to an sufficiently advanced textbook on numerical methods, e.g. Ref. [2].

where H is the Hamiltonian of the system. The solution to this equation is just,

$$\psi = e^{-iHt/\hbar}\psi_0 = \sum_{n=0}^{\infty} \frac{(-iHt/\hbar)^n}{n!}\psi_0, \tag{3.18}$$

which is because H is hermitian an unitary transformation. To compute this exponent we could simply compute a large number of terms from the series expansion. But aside from the obvious inefficiency of this method it is also not unitary. In many cases we can simplify this matrix exponential considerably by splitting the Hamiltonian in two parts $H = A + B$ in such a way that we can compute the matrix exponent of A and B easily. Care should be taken that A and B are also hermitian, so that the matrix exponents of A and B are again unitary. However in general $e^{A+B} \neq e^A e^B$. This can be easily shown by using the power series expansions to second order

$$\begin{aligned} e^{A+B} &= 1 + (A+B) + \frac{1}{2}(A^2 + AB + BA + B^2) + \ldots, \\ e^A e^B &= (1 + A + \frac{1}{2}A^2 + \ldots)(1 + B + \frac{1}{2}B^2 + \ldots) = 1 + (A+B) + \frac{1}{2}(A^2 + 2AB + B^2)\ldots, \end{aligned} \tag{3.19}$$

only when A and B commute $e^{A+B} = e^A e^B$ is exact. The method we just described is called the first order Suzuki-Trotter method. A second order method using this procedure is obtained easily to be

$$e^{A+B} \approx e^{A/2} e^B e^{A/2}, \tag{3.20}$$

whose correctness can easily be checked by considering the Taylor expansion. For higher order Suzuki-Trotter methods the problem becomes more difficult. A fourth order method is given by [4]

$$e^{A+B} = e^{A/2} e^{B/2} e^{C(A,B)} e^{B/2} e^{A/2}, \tag{3.21}$$

where,

$$C(A,B) = [A + 2B, [A,B]]/24. \tag{3.22}$$

It can be proven that this indeed has an fourth order error bound. To compute the exponent of the double commutator we simply decompose $C(A,B)$ into a series, $C(A,B) = \sum_{i=1}^{r} C_i$ and invoke the first order Suzuki-Trotter formula,

$$e^{C(A,B)} = \prod_{i=1}^{r} e^{C_i}, \tag{3.23}$$

which leaves the fourth order behaviour intact [4]. The choice of decomposition will depend on the particular $C(A,B)$. It is also not a priory clear if the fourth order method will be faster then the second order method. Even though the fourth order method is of higher order, it also does more computations per time step then the second order method. In practice though it turns out that for most applications the fourth order method is significantly more efficient then the second order method.

Bibliography

[1] E. Issacson and H.B. Keller, Analysis of numerical methods, John Wiley and Sons, ISBN: 0471428655 (1966).

[2] Richard Burden and J. Faires, Numerical Analysis (seventh edition), Brooks Cole, ISBN: 0534382169 (2000).

[3] P. Prelovsek, *Numerical Study of the Conductivity in the Vicinity of Mobility Edges*, Phys. Rev. Lett. (40), 1596 (1978).

[4] H. de Raedt, *"Product formula algorithms for solving the time dependent Schrödinger equation"*, Comput. Phys. Rep. 7, 1(1987).

Chapter 4

Numerical results

As part of the master thesis a numerical simulation tool was developed to study persistent currents in small rings. The tool was developed incrementally, starting out with a basic Hamiltonian and then expanding it step by step until arriving at the full Hamiltonian. At each step the correctness of the implementation was thoroughly tested. The numerical method we used is used is the Suzuki-Trotter method described in section 3.3. In the following chapter this step-by-step development will be given in detail. Following this we shall use the numerical tool to analyze the properties of various rings and we will compare the results to theory and experiment.

4.1 Single electron ring without impurities

We start with the most simple Hamiltonian, namely the tight-binding Hamiltonian with one spinless electron and no impurities,

$$H = -V \sum_{i=1}^{N} (c_i^\dagger c_{i+1} e^{2i\pi\phi/N\phi_0} + e^{-2i\pi\phi/N\phi_0} c_{i+1}^\dagger c_i), \tag{4.1}$$

we treated this system analytically in section 2.3.

4.1.1 The time step operator

To simulate the system described by Hamiltonian (4.1) we use the second order Suzuki-Trotter method detailed in section(3.3). The reason for not choosing a fourth order method is that we are going to make many small changes to the Hamiltonian and the fourth order method would complicate the development considerably. Hamiltonian (4.1) can be split in two block diagonal matrices with identical 2×2

matrices on the diagonal,

$$H = -\underbrace{\begin{pmatrix} 0 & t & 0 & \dots & \dots & \dots & 0 \\ t^* & 0 & 0 & \ddots & & & \vdots \\ 0 & 0 & 0 & t & \ddots & & \vdots \\ \vdots & \ddots & t^* & 0 & 0 & \ddots & \vdots \\ \vdots & & \ddots & 0 & 0 & t & 0 \\ \vdots & & & \ddots & t^* & 0 & 0 \\ 0 & \dots & \dots & \dots & 0 & 0 & \ddots \end{pmatrix}}_{A} - \underbrace{\begin{pmatrix} 0 & 0 & 0 & \dots & \dots & \dots & 0 \\ 0 & 0 & t & \ddots & & & \vdots \\ 0 & t^* & 0 & 0 & \ddots & & \vdots \\ \vdots & \ddots & 0 & 0 & t & \ddots & \vdots \\ \vdots & & \ddots & t^* & 0 & 0 & 0 \\ \vdots & & & \ddots & 0 & \ddots & \\ 0 & \dots & \dots & \dots & 0 & & \ddots \end{pmatrix}}_{B}, \tag{4.2}$$

where $t = Ve^{i2\pi\phi/N\phi}$. Also implied here is that the first and the last element of the Hamiltonian work on the same lattice site (because we have a ring). Now we are going to calculate $e^{iH\tau}$ which is the time step operator. This operator takes our system from the state $\psi(T)$ at time T to the state $\psi(T+\tau)$. The second-order Suzuki-Trotter method gives the approximation $e^{iH\tau} \approx e^{iB\tau/2}e^{iA\tau}e^{iB\tau/2}$. We only need to consider the exponent of 2×2 matrices $\tilde{H}$ that are on the diagonal,

$$\tilde{H} = \begin{pmatrix} 0 & e^{2i\pi\phi/N\phi_0} \\ e^{-2i\pi\phi/N\phi_0} & 0 \end{pmatrix}. \tag{4.3}$$

The exponent of this matrix is,

$$\begin{aligned} e^{-iV\tau\tilde{H}} &= \sum_{n=0}^{\infty} \frac{(-iV\tau)^n}{n!} \begin{pmatrix} 0 & e^{2i\pi\phi/N\phi_0} \\ e^{-2i\pi\phi/N\phi_0} & 0 \end{pmatrix}^n \\ &= \sum_{n=0}^{\infty} \frac{(-1)^n (V\tau)^{2n}}{2n!} I - i \sum_{n=1}^{\infty} \frac{(-1)^{n-1}(V\tau)^{2n-1}}{(2n-1)!} \begin{pmatrix} 0 & e^{2i\pi\phi/N\phi_0} \\ e^{-2i\pi\phi/N\phi_0} & 0 \end{pmatrix} \\ &= \cos(V\tau)I - i\sin(V\tau) \begin{pmatrix} 0 & e^{2i\pi\phi/N\phi_0} \\ e^{-2i\pi\phi/N\phi_0} & 0 \end{pmatrix}, \end{aligned} \tag{4.4}$$

with I the identity matrix. It is straightforward to implement this method in a computer program.

4.1.2 The current operator

To be able to calculate the current I in the ring for some eigenstate ψ we need to derive a current operator for Hamiltonian (4.1). The current operator is in general given by[1]

$$j = \frac{\partial P}{\partial t} = i[H, P], \tag{4.5}$$

where P denotes the polarization which is given by

$$P = \sum_k R_k n_{k,\sigma}, \tag{4.6}$$

where R_k is the position vector and $n_{k,\sigma} \equiv c^\dagger_{k,\sigma} c_{k,\sigma}$ is the counting operator. The evaluation of the commutator of equation (4.5) is straightforward but lengthy. To simplify notation we use the notation $t = Ve^{i2\pi\phi/N\phi}$. We start by evaluating the first term of the commutator,

$$HP = -\sum_i \sum_\sigma \sum_{\substack{k\neq i \\ k\neq i+1}} (c^\dagger_{i,\sigma}c_{i+1,\sigma}t + c^\dagger_{i+1,\sigma}c_{i,\sigma}t^*)R_k c^\dagger_{k,\sigma}c_{k,\sigma} - \sum_i \sum_\sigma (c^\dagger_{i,\sigma}c_{i+1,\sigma}t + c^\dagger_{i+1,\sigma}c_{i,\sigma}t^*)R_i c^\dagger_{i,\sigma}c_{i,\sigma} -$$
$$\sum_i \sum_\sigma (c^\dagger_{i,\sigma}c_{i+1,\sigma}t + c^\dagger_{i+1,\sigma}c_{i,\sigma}t^*)R_{i+1} c^\dagger_{i+1,\sigma}c_{i+1,\sigma}.$$

Similarly the second term of the commutator is

$$PH = -\sum_i \sum_\sigma \sum_{\substack{k \neq i \\ k \neq i+1}} R_k c^\dagger_{k,\sigma} c_{k,\sigma} (c^\dagger_{i,\sigma} c_{i+1,\sigma} t + c^\dagger_{i+1,\sigma} c_{i,\sigma} t^*) -$$

$$\sum_i \sum_\sigma R_i c^\dagger_{i,\sigma} c_{i,\sigma} (c^\dagger_{i,\sigma} c_{i+1,\sigma} t + c^\dagger_{i+1,\sigma} c_{i,\sigma} t^*) - \sum_i \sum_\sigma R_{i+1} c^\dagger_{i+1,\sigma} c_{i+1,\sigma} (c^\dagger_{i,\sigma} c_{i+1,\sigma} t + c^\dagger_{i+1,\sigma} c_{i,\sigma} t^*).$$

Note that the standard fermion commutation relations given by

$$\begin{aligned} \{c_k, c^\dagger_p\} &= \delta(k-p) \\ \{c^\dagger_k, c^\dagger_p\} &= 0 \\ \{c_k, c_p\} &= 0. \end{aligned} \tag{4.7}$$

imply that the first term of PH and HP cancel each other, writing out the commutator gives

$$[H, P] = -\sum_i \sum_\sigma R_i (c^\dagger_{i,\sigma} c_{i+1,\sigma} t (c^\dagger_{i,\sigma} c_{i,\sigma} - c_{i,\sigma} c^\dagger_{i,\sigma}) + (c_{i,\sigma} c^\dagger_{i,\sigma} - c^\dagger_{i,\sigma} c_{i,\sigma}) c^\dagger_{i+1,\sigma} c_{i,\sigma} t^*) -$$

$$V \sum_i \sum_\sigma R_{i+1} (c^\dagger_{i+1,\sigma} c_{i,\sigma} t^* (c^\dagger_{i+1,\sigma} c_{i+1,\sigma} - c_{i+1,\sigma} c^\dagger_{i+1,\sigma}) + (c_{i+1,\sigma} c^\dagger_{i+1,\sigma} - c^\dagger_{i+1,\sigma} c_{i+1,\sigma}) c^\dagger_{i,\sigma} c_{i+1,\sigma} t).$$

Applying again the commutation relations (4.7) and inserting the result in equation (4.5) gives the current operator

$$\begin{aligned} j &= -iV \sum_i \sum_\sigma R_i (-c^\dagger_{i,\sigma} c_{i+1,\sigma} t + c^\dagger_{i+1,\sigma} c_{i,\sigma} t^*) - iV \sum_i \sum_\sigma R_{i+1} (-c^\dagger_{i+1,\sigma} c_{i,\sigma} t^* + c^\dagger_{i,\sigma} c_{i+1,\sigma} t) \\ &= -iV \sum_i \sum_\sigma (R_{i+1} - R_i)(c^\dagger_{i,\sigma} c_{i+1,\sigma} t - c^\dagger_{i+1,\sigma} c_{i,\sigma} t^*). \end{aligned}$$

In our case we take $(R_{i+1} - R_i) = 1$ and thus the final result is

$$j = -iV \sum_i \sum_\sigma (c^\dagger_{i,\sigma} c_{i+1,\sigma} e^{i2\pi\phi/N\phi} - e^{-i2\pi\phi/N\phi} c^\dagger_{i+1,\sigma} c_{i,\sigma}). \tag{4.8}$$

4.1.3 Numerical calculations

The last ingredient for our program is a tool for computing the eigenstates of a system with N sites and flux ϕ. For this we will use the LAPACK[2] numerical library. We will also use it to check the results of the time step operator by doing an exact diagonalization of the Hamiltonian.

Now everything is in place to do some calculations. We start with the case $N = 3$ and use this as a starting point to show the correctness of the program. We can calculate the eigenvalues and eigenvectors for $N = 3$ easily by hand, this we can then use as a check for the results from LAPACK. The eigenvalues were calculated analytically in section 2.3, where according to equation (2.25),

$$E_n = -2V \cos\left(\frac{2\pi}{N}(n + \phi/\phi_0)\right). \tag{4.9}$$

We now start with the case $\phi = 0$. Then the eigenvalues calculated by diagonalizing Hamiltonian (4.1) by hand are $\{-2, 1, 1\}$ and the corresponding eigenvectors are

$$\begin{pmatrix} 1 \\ 1 \\ 1 \end{pmatrix}, \quad \begin{pmatrix} -1 \\ 0 \\ 1 \end{pmatrix}, \quad \begin{pmatrix} -1 \\ 1 \\ 0 \end{pmatrix}. \tag{4.10}$$

When we take ϕ to be non-zero and repeat the manual calculation of the eigenvalues and eigenvectors, we find the eigenvalues to be

$$\{-2\cos(2\pi\phi/N\phi_0), \quad -2\cos(\frac{2\pi}{3}(\phi/\phi_0+1)), \quad -2\cos(\frac{2\pi}{3}(\phi/\phi_0-1))\}, \tag{4.11}$$

and the corresponding eigenvectors now are

$$\begin{pmatrix}1\\1\\1\end{pmatrix}, \quad \begin{pmatrix}-1-i\sqrt{3}\\-1+i\sqrt{3}\\2\end{pmatrix}, \quad \begin{pmatrix}-1+i\sqrt{3}\\-1-i\sqrt{3}\\2\end{pmatrix}. \tag{4.12}$$

Notice that when we take $\phi \to 0$ the eigenvalues for the case with finite ϕ will be identical to those of $\phi = 0$ but the eigenstates are totally different. As we shall see below at $\phi = 0$ a discontinuous jump in the current for some of the eigenstates. In Figs.4.1(a)-(d) we plot the current for all eigenstates as a function of ϕ/ϕ_0, the continuous line is from the analytical expression equation (2.25) we derived in section 2.3,

$$I_n = -\frac{2eV}{N\hbar}\sin(\frac{2\pi}{N}[n+\phi/\phi_0]), \tag{4.13}$$

and the triangles are numerical results calculated with the program. These results from the numerical tool are indeed consistent with the theoretical values, tests for larger systems show the same consistency with theory.

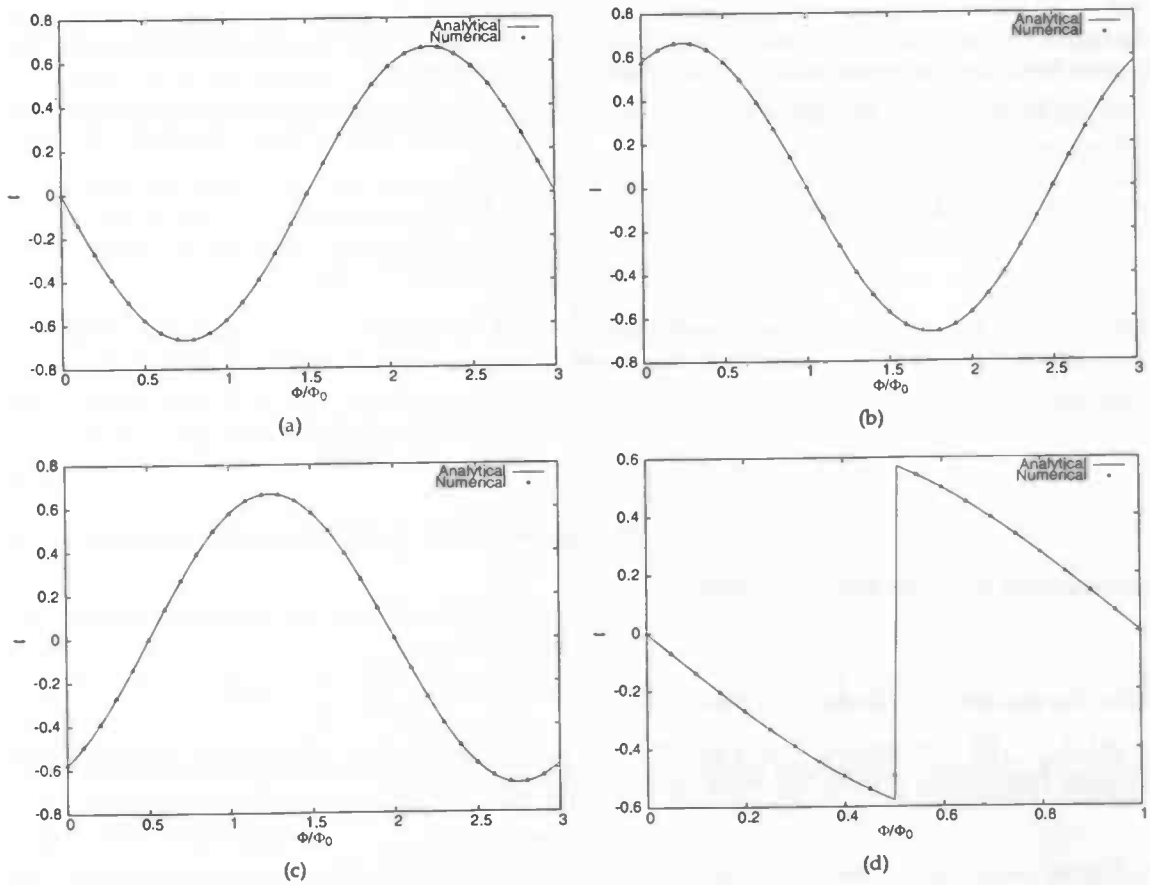

Figure 4.1: *The currents in the various (eigen) states with in (a) the first eigenstate, (b) the second eigenstate, (c) the third eigenstate and (d) the ground state.*

4.2 Many-electron systems

We will now extend our program to the many-electron case. The many-electron version of Hamiltonian (4.1) for N electrons when neglecting electron-electron interactions is just

$$H = -V \sum_{e=1}^{N_e} \sum_{i}^{N} \sum_{\sigma} (c^{\dagger}_{e,i,\sigma} c_{e,i+1,\sigma} + c^{\dagger}_{e,i+1,\sigma} c_{e,i,\sigma}). \tag{4.14}$$

An N_e-electron wave function can be written as a product of N_e single electron wave functions. To do this there are two important facts which have to be taken in to account when constructing the wave function:

- Electrons are indistinguishable particles, thus one can't track *which* particle is in a certain state but only say that *a* particle is in that state.
- Electrons are fermions, thus no two electrons can be in the same state.

Take for instance the case of two electrons in a two level system with energy levels ϵ_a and ϵ_b. Using the considerations detailed above we construct a wave function for this case as

$$\Psi(1,2) = \frac{1}{\sqrt{2}}(\psi_a(x_1)\psi_b(x_2) - \psi_a(x_2)\psi_b(x_1)), \tag{4.15}$$

with $\psi_a(x)$ and $\psi_b(x)$ the single particle wave functions belonging to states ϵ_a respectively ϵ_b, note that the wave function disappears when both particles are in the same state.

In general an N_e-particle Fermionic wave function is given by an alternating sum of the permutations of the states

$$\Psi(1,2,\ldots,n) = \sum_{P} (-1)^P P\psi_a(1)\psi_b(2)\cdots\psi_n(n) \tag{4.16}$$

$$= \psi_a(1)\psi_b(2)\cdots\psi_n(n) - \psi_a(2)\psi_b(1)\cdots\psi_n(n) + \cdots, \tag{4.17}$$

where P stands for the permutation operator and $(-1)^P$ is -1 for odd permutations and $+1$ for even permutations. Another way to write wave function(4.17) is via a Slater determinant defined by

$$\Psi(1,2,\ldots,n) = \frac{1}{\sqrt{n!}} \begin{vmatrix} \psi_a(1) & \psi_a(2) & \cdots & \psi_a(n) \\ \psi_b(1) & \psi_b(2) & \cdots & \psi_b(n) \\ \vdots & \vdots & \ddots & \vdots \\ \psi_n(1) & \psi_n(2) & \cdots & \psi_n(n) \end{vmatrix}, \tag{4.18}$$

or alternatively in a more compact notation,

$$\Psi(1,2,\ldots,n) = \mathcal{A}\psi_a\psi_b\cdots\psi_n, \tag{4.19}$$

where $\mathcal{A}$ is the anti-symmetrize operation.

Let $\Psi(1,2,\cdots,n) = \det\{\psi_a\psi_b\cdots\psi_n\}$ and $\Phi(1,2,\cdots,n) = \det\{\Phi_a\Phi_b\cdots\Phi_n\}$ be the N particle wave functions. The overlap of these two wave functions is given by [4, 5]

$$\langle\Phi|\Psi\rangle = D\det\{\mathcal{O}\}, \tag{4.20}$$

where D is a normalization constant and $\mathcal{O}$ is the overlap matrix defined by

$$\mathcal{O}_{\alpha\beta} = \langle\Phi_\alpha|\psi_\beta\rangle \tag{4.21}$$

The matrix elements of a one body operator $T = \sum_{\alpha=1}^{n} t_\alpha$, with t_α an operator that only acts on particle α, is given by

$$\langle \Phi | T \Psi \rangle = \sum_{\alpha=1}^{n} \langle \mathcal{A}\Phi_a \Phi_b \cdots \Phi_n | t_\alpha \mathcal{A}\psi_a \psi_b \cdots \psi_n \rangle = \sum_{\alpha} \langle t_\alpha \Phi_a \Phi_b \cdots \Phi_n | \mathcal{A}\psi_a \psi_b \cdots \psi_n \rangle. \tag{4.22}$$

Thus the effect of the operator t_α is to replace the α'th row of (4.20) with

$$\mathcal{O}_{\alpha\beta} = \langle t_\alpha \Phi_\alpha | \psi_\beta \rangle = \langle \Phi_\alpha | t_\alpha \psi_\beta \rangle. \tag{4.23}$$

Equation (4.22) can be evaluated by means of a cofactor expansion, let $A = a_{ij}$ be a $n \times n$ matrix then,

$$\det\{A\} = \sum_{ij} a_{ij} c_{ij}, \tag{4.24}$$

where c is the so called cofactor matrix determined by,

$$c_{ij} = a_{ji}^{-1} \det\{A\}. \tag{4.25}$$

Using this result in equation (4.22) gives the final result

$$\langle \Phi | T \Psi \rangle = \sum_{\alpha\beta} \langle \Phi_\alpha | t_\alpha \psi_\beta \rangle c_{\alpha\beta} = \langle \Phi | \Psi \rangle \sum_{\alpha\beta} \langle \Phi_\alpha | t_\alpha \psi_\beta \rangle \mathcal{O}_{\beta\alpha}^{-1*} \tag{4.26}$$

Now to return to our system. We have a N particle system in the ground state with $\Psi(1, 2, \cdots, N) = \mathcal{A}\psi_a \psi_b \cdots \psi_n$, where ψ_i are the orthogonal single particle wave functions. Because the Hamiltonian (4.14) only has single electron terms, the time step operator in this case is just a product of N single particle time step operators (identical to one derived for the one-electron case). Each time step operator works on a different single particle wave function ψ.

To evaluate the current we note that the current is a single particle operator and thus the expectation value of the current can be evaluated from equation (4.26). Note that the ψ's are orthogonal and thus the overlap matrix in this case is just the unity matrix,

$$\langle \Psi | J \Psi \rangle = \sum_{\alpha=1}^{n} \langle \psi_\alpha | J \psi_\alpha \rangle. \tag{4.27}$$

These results allow us to extend our simulation to the many-electron case with little effort. We can almost treat it as N_e single particle systems.

4.3 many-electron ring with disorder

The Hamiltonian in the case with disorder reads

$$H = -V \sum_{e=1}^{N_e} \left[\sum_{i}^{N} \sum_{\sigma} (c_{e,i,\sigma}^{\dagger} c_{e,i+1,\sigma} + c_{e,i+1,\sigma}^{\dagger} c_{e,i,\sigma}) + \sum_{i} W_i n_i \right], \tag{4.28}$$

where W_i is the disorder potential at each site. The current operator remains unchanged by the addition of the impurity term because the impurity term only has diagonal components and therefore commutes with the counting operator.

The most obvious way to construct the time step operator is to split the Hamiltonian in two parts A and B, where A is the Hamiltonian without impurities and B is the impurity term, allowing us to recycle the result from our previous analysis. This is however not the most efficient splitting[3], but as our splitting is easier to adapt to further additions to the Hamiltonian we will opt for this less efficient splitting.

In Figs. 4.2(a)-(d) we present results for different lattice sizes. We plot the error of the time-evolution operator against time for two time steps $\tau = 0.1$ and $\tau = 0.05$ and take $\phi/\phi_0 = 0.25$. The impurities are generated with a random number generator, the strength of the perturbations is between $-\frac{1}{2} \leq W_i \leq \frac{1}{2}$. The initial wave function is also chosen to be random.

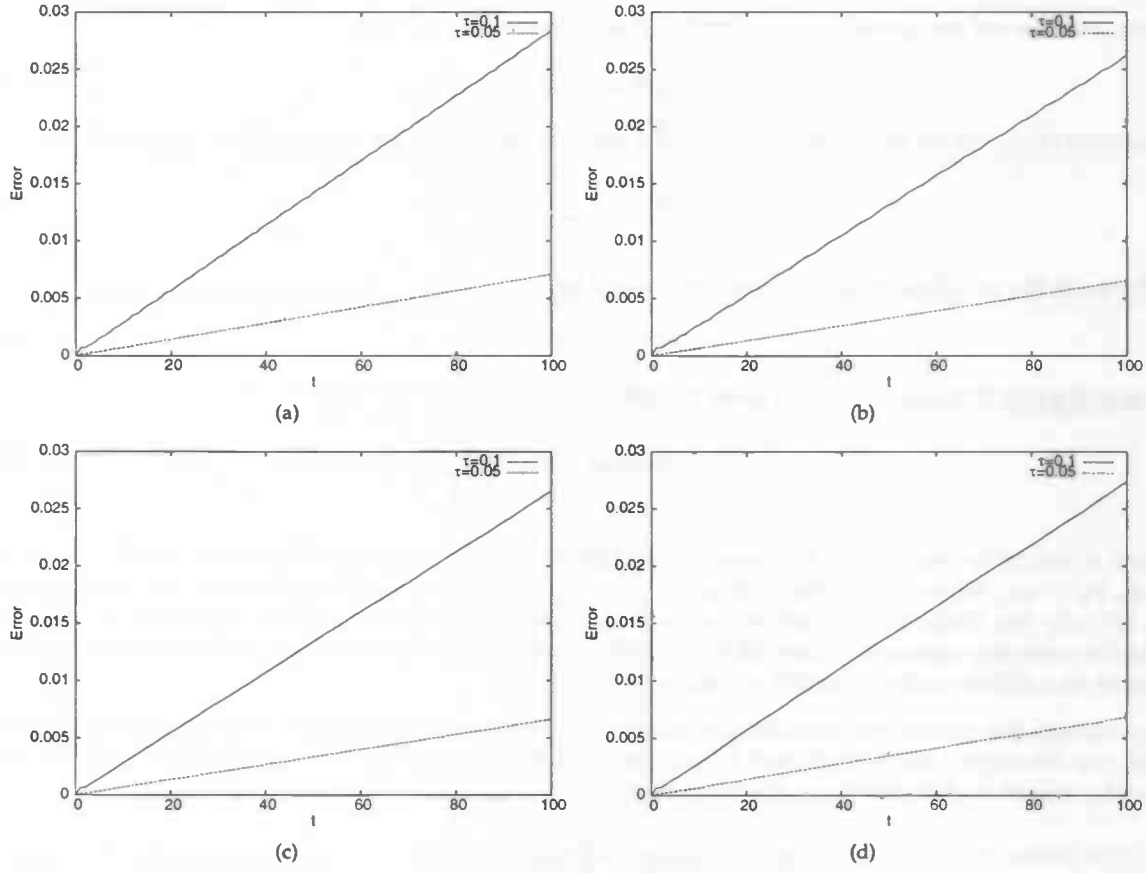

Figure 4.2: *Time evolution of the error in the wave function for (a)* $N = 3$*, (b)* $N = 4$*, (c)* $N = 99$ *and (d)* $N = 100$.

Notice that the error reduces with a factor four when we take τ to be a factor two smaller, which is consistent with what we expect from a second order Suzuki-Trotter algorithm.

4.3.1 The effect of disorder

The presence of a random disordering potential induces the phenomenon of localization of which the basic features were discussed in section 2.4.1. The basic features are also present in our simulation. For instance when there is a random potential present in the ring, the eigenstates will be localized. In the Figs. 4.3(a) and (b) the density distribution of two eigenstates is plotted for a number of disordering strengths. The eigenstates are labeled according to their energy in increasing order (eigenstate 1 is lowest in energy and eigenstate 200 is highest). The disorder strength W determines the maximum/minimum of the potential according to $-W/2 \leq W_i \leq W/2$.

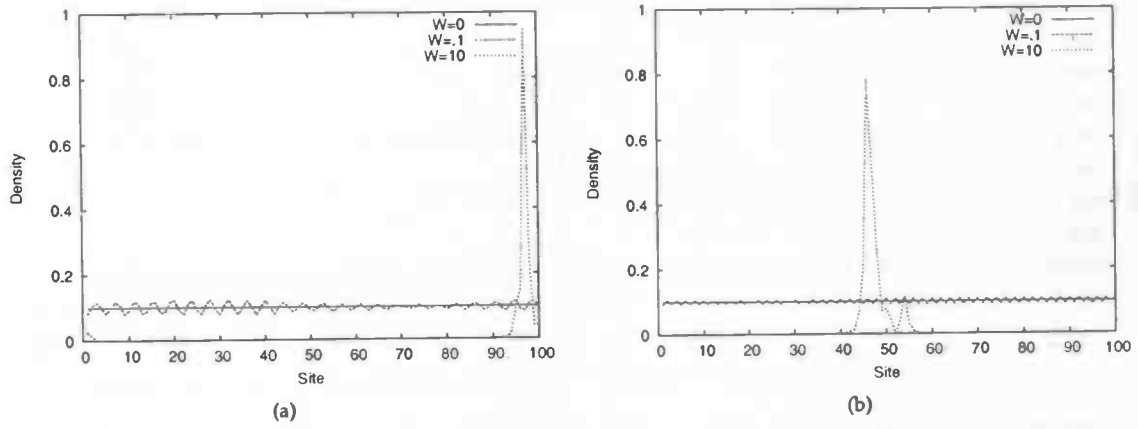

Figure 4.3: *Electron density for* $N = 100$ *and* $\phi/\phi_0 = 0.2$ *for (a) eigenstate 50 and (b) eigenstate 100.*

For $W = 0$ the state is not localized and for small W the localization length is larger then the ring. This feature is present in the figures above as these states are (nearly) uniformly distributed over the ring. In the case of large W the localization length becomes smaller than the ring and these states are clearly localized in some region, as shown in Figs. 4.3(a) and (b).

Another basic feature is the behaviour of the second moment $< x^2(t) > - < x(t) >^2$ of $\psi(\vec{x}, t)$. For a localized state the second moment converges to[6]

$$\lim_{t\to\infty} < x^2(t) > - < x(t) >^2 = 2\xi^2, \qquad W \gg V \tag{4.29}$$

where ξ is the localization length. For any finite W all states are localized, but in the limit of small W the localization length will be so large that in effect electrons will behave like free particles. The second moment in this case is [6]

$$< x^2(t) > - < x(t) >^2 = t^2, \qquad W = 0, \tag{4.30}$$

where t is the time. Of course these two limits of the second moment are only valid if boundary effects can be neglected. In the case of our ring that means that in the localized regime the localization length must be smaller then the ring.

In Figs. 4.4(a) and (b) the phenomenon of localization by plotting the time evolution of the second moment for various W in a ring of $N = 1000$ sites. As initial wave function we put one electron in the middle of the ring. The magnetic field will be switched off, thus $\phi = 0$. Clearly these plots are consistent with their expected asymptotic behaviour. In paragraph 2.4.1 we discussed the effect of disorder on the current. An estimate of the average current in the weak disorder limit ($W \ll 2\pi V$) for a half-filled ring with $\phi/\phi_0 = 0.25$ was also made. We found that

$$\bar{I} = \frac{1}{2} I_0 e^{-L/\xi}, \tag{4.31}$$

with $\xi = 105a\frac{V^2}{W^2}$, a the lattice spacing and W the maximum amplitude of the random impurity potential. In Figs. 4.5(a) and (b) we plot the numerically calculated currents together with the estimate. The average current was calculated for a ring with $V = 1$ by averaging the current over a 100 different random impurity distributions. The estimate agrees very well with the numerical results for small W but as W increases the estimate looses its accuracy.

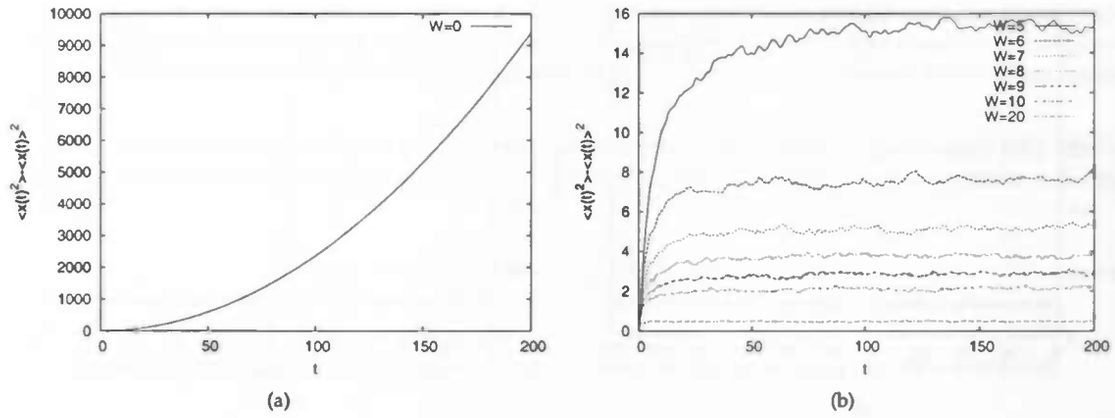

Figure 4.4: *Time evolution of the second moment for* $N = 1000$ *with (a)* $W = 0$ *and (b)* $5 \leq W \leq 10$.

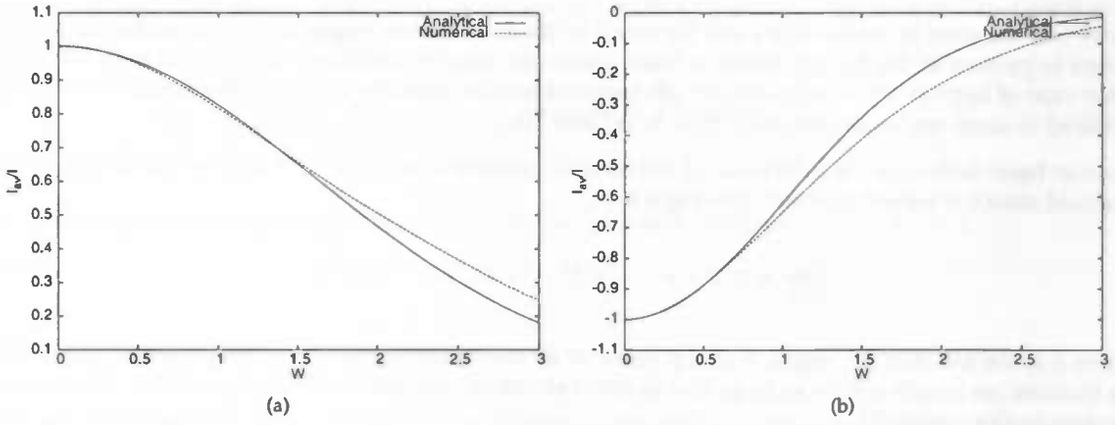

Figure 4.5: *The average current in the weak disorder limit with* $\phi/\phi_0 = 0.25$ *and for lattice sizes (a)* $N = 20$ *and (b)* $N = 50$.

4.4 Making contact with experiment

Until now the results from our simulation tool could not be directly translated into experimental quantities. We defined all constants in a convenient way (like setting $V = 1$). For the tight-binding model this is adequate to discover the main features of the system. But to do quantitative predictions that can be verified by experiment we need to map the Hamiltonian describing the continuum case onto the tight-binding Hamiltonian. This will allow us to redefine all the constants in such a way that the that we can simulate the continuum problem using our implementation of the tight-binding model. The continuum Hamiltonian is given by

$$H = \frac{1}{2m}(P - e\vec{A}/c)^2 + \frac{e\hbar}{mc}\vec{B}\cdot\vec{S} + V(x), \tag{4.32}$$

where $P = -i\hbar\frac{\partial^2}{\partial x^2}$ is the momentum operator, $\vec{A}$ the vector potential, $\vec{B}$ the magnetic field which is related to $\vec{A}$ by $\vec{B} = \vec{\nabla} \times \vec{A}$ and $\vec{S}$ the spinors which are related to the Pauli spin matrices σ by $\vec{S} = \vec{\sigma}/2$. The second term in equation (4.32) is called the Zeeman term.

Using $\phi = \pi R^2 B$ and $L = 2\pi R$ for a ring of radius R we find

$$B = \frac{4\pi^2}{L^2}\phi. \tag{4.33}$$

These relations allow us to rewrite equation (4.32) as

$$H = \frac{1}{2m}[(P + (e\vec{A}/c)]^2 + \frac{2e\hbar\pi}{mcL^2}\phi\sigma_z + V(x). \tag{4.34}$$

To make contact between equation (4.34) and the tight-binding model, we need to rewrite equation (4.34) in terms of dimensionless quantities. A convenient choice of units is to use the Fermi level as a basis for our new units. We use the following units

$$\text{Energy} : E \to [E_f], \quad \text{Momentum} : k \to [k_F], \quad \text{Length} : x \to [\lambda_f], \quad \text{Flux} : \phi \to [\phi_0]. \tag{4.35}$$

From section 2.2 we know that the effect of the vector potential is to add a phase factor e^{ig} to the wave function ψ. We can thus temporarily remove it from our equation and add the phase factor later at the end. We now write equation (4.34) in the new units [1]

$$\begin{aligned} H &= -\frac{\hbar^2}{2m}\frac{1}{\lambda_f^2}\frac{\partial^2}{\partial x'^2} + \frac{e\hbar}{mc}\frac{\phi_0}{\lambda_F^2}\frac{2\pi\phi'\sigma_z}{L'^2} + E_f V' \\ &= -\frac{E_f}{(2\pi)^2}\frac{\partial^2}{\partial x'^2} + \frac{4\pi^2\hbar^2}{mL'^2}\frac{1}{\lambda_F^2}\phi'\sigma_z + E_f V' \\ &= -\frac{E_f}{(2\pi)^2}\frac{\partial^2}{\partial x'^2} + \frac{2E_f}{L'^2}\phi'\sigma_z + E_f V' \\ &= E_f \hat{H} \end{aligned} \tag{4.36}$$

Equation (4.36) has formal solution

$$\psi(x,t) = e^{iHt/\hbar}\psi(x,0) = e^{i\hat{H}E_f t/\hbar}\psi(x,0). \tag{4.37}$$

This allows us to one more change of variables we redefine t as an dimensionless quantity $t \to E_f t/\hbar$. Now we are going to discretize equation (4.36). We use the central difference formula

$$\frac{\partial^2}{\partial x^2} \approx \frac{1}{\delta^2}(c_i^\dagger c_{i+1} - 2c_i^\dagger c_i + c_i^\dagger c_{i-1}), \tag{4.38}$$

where δ is the distance between two coordinates x_i and x_{i+1}. Inserting this in equation (4.36) gives

$$\begin{aligned} \hat{H} &= -\sum_i \left(\frac{1}{(2\pi\delta)^2}(c_i^\dagger c_{i+1} - 2c_i^\dagger c_i + c_i^\dagger c_{i-1}) - \frac{2\phi}{L^2}c_i^\dagger\sigma_z c_i - W_i c_i^\dagger c_i\right) \\ &= -\sum_i \left(\frac{1}{4\pi^2\delta^2}(c_i^\dagger c_{i+1} + c_i^\dagger c_{i-1}) - \frac{2\phi}{L^2}c_i^\dagger\sigma_z c_i - (W_i + \frac{1}{2\pi^2\delta^2})c_i^\dagger c_i\right). \end{aligned} \tag{4.39}$$

As a final step we are going to add the phase factor e^{ig} which we omitted when we removed the vector potential from the Hamiltonian. In section 2.2 we calculated the total phase shift Δ between electrons traveling clockwise and anti-clockwise around the ring which was given by equation (2.12):

$$\Delta = 2\pi\frac{\phi}{\phi_0}, \tag{4.40}$$

this translates into a phase shift per "hop" of $e^{\pm 2\pi i\phi/\phi_0 N}$, where the sign is determined by the direction of the electron movement. We are now ready to write the final result which is just a tight-binding Hamiltonian

$$\hat{H} = -\sum_i \left(\frac{1}{4\pi^2\delta^2}(c_i^\dagger c_{i+1}e^{2\pi i\phi/N} + e^{-2\pi i\phi/N}c_i^\dagger c_{i-1}) - \frac{2\phi}{L^2}c_i^\dagger\sigma_z c_i - (W_i + \frac{1}{2\pi^2\delta^2})c_i^\dagger c_i\right). \tag{4.41}$$

[1] In the following will put an accent on a variable to indicate that it is in the new units.

To do an accurate simulation we need to have a reasonable number of sampling points per Fermi wavelength, typically we take 10 lattice points per Fermi wavelength. Note that in this situation we also have lattice points between the atoms but that in our model, all impurities are localized at sites that contain an atom.

To be able to interpret the results of the current operator, which we calculated previously (the result is in equation (4.8)), we need to repeat the derivation using our new units. The current operator is defined to be

$$j = -\frac{ie}{\hbar}[H, P] = -\frac{ie}{\hbar}[H, \sum_i R_i n_i], \tag{4.42}$$

with P the polarization and R_i the position vector. We rewrite this in terms of our new variables,

$$j = -\frac{ie}{\hbar}[H, \sum_i R_i n_i] = -\frac{ieE_F}{\hbar}[\frac{H}{E_f}, \sum_i R_i n_i] \tag{4.43}$$

where we have used that n_i is a density with unit 1/length so that the units of R_i and n_i cancel each other. The current operator reads

$$j = -\frac{ie}{\hbar}E_f \delta V \sum_i \sum_\sigma (c^\dagger_{i,\sigma} c_{i+1,\sigma} e^{i2\pi\phi/N\phi} - e^{-i2\pi\phi/N\phi} c^\dagger_{i+1,\sigma} c_{i,\sigma}) = \frac{eE_F}{\hbar}\hat{j} \tag{4.44}$$

where $\hat{j}$ is the dimensionless current operator. In the derivation we used $(R_{i+1} - R_i) = \delta$.

4.4.1 Effects of the Zeeman term

Before we compare the output of our numerical simulations with experiment we first have to investigate what the effect of the Zeeman term is on the persistent current. Because the term scales with L^2 we expect the effects to be noticeable only when either the rings are very small or when the magnetic field is very large. The Zeeman term adds a potential energy term which is *different* for spin up as for spin down. When we consider an N_e electron ground state, the N_e states that are lowest in energy are filled. When the Zeeman term is not present all states are doubly degenerate in energy (one state with spin up and the other with spin down). The effect of the Zeeman term is that there will be a preference for one spin direction, thus the sequence in which states are filled up in the ground state may will be altered if the effect is large enough.This will have dramatic effect on the persistent current, which will loose it's ϕ_0 periodicy. In its extreme limit the sequence of states for a system of N sites will be altered such that the states with the preferred spin direction will occupy the first N states which are lowest in energy.

In Figs. 4.6(a)-(c) we present plots of the persistent current for various gold lattices. We used $W = 0$ and $N_e = N$. The effect is (as expected) the most profound in the case $N = 3$. Clearly visible is also that when ϕ becomes large enough that the system will be split completely between negative energy states with spin down and with positive energy states having spin up. When this splitting is complete, then in the half-filled case the current will vanishes[2]. When we add disorder the behaviour is similar.

In our examples the effect of the Zeeman term is very large. However, the magnetic fields involved in these examples are also extremely large. For instance the field strength necessary to create a flux of $\phi/\phi_0 = 1$ in a gold ring with $N = 100$ is $B = 4\pi/L^2 = 79.3\,T$. In experiment field strengths of the order of mT are used. Therefore we will omit the Zeeman term in the rest of our simulations.

[2]For $N = 100$this is not visible in the plots, but was found to be at $\phi/\phi_0 \approx 245$

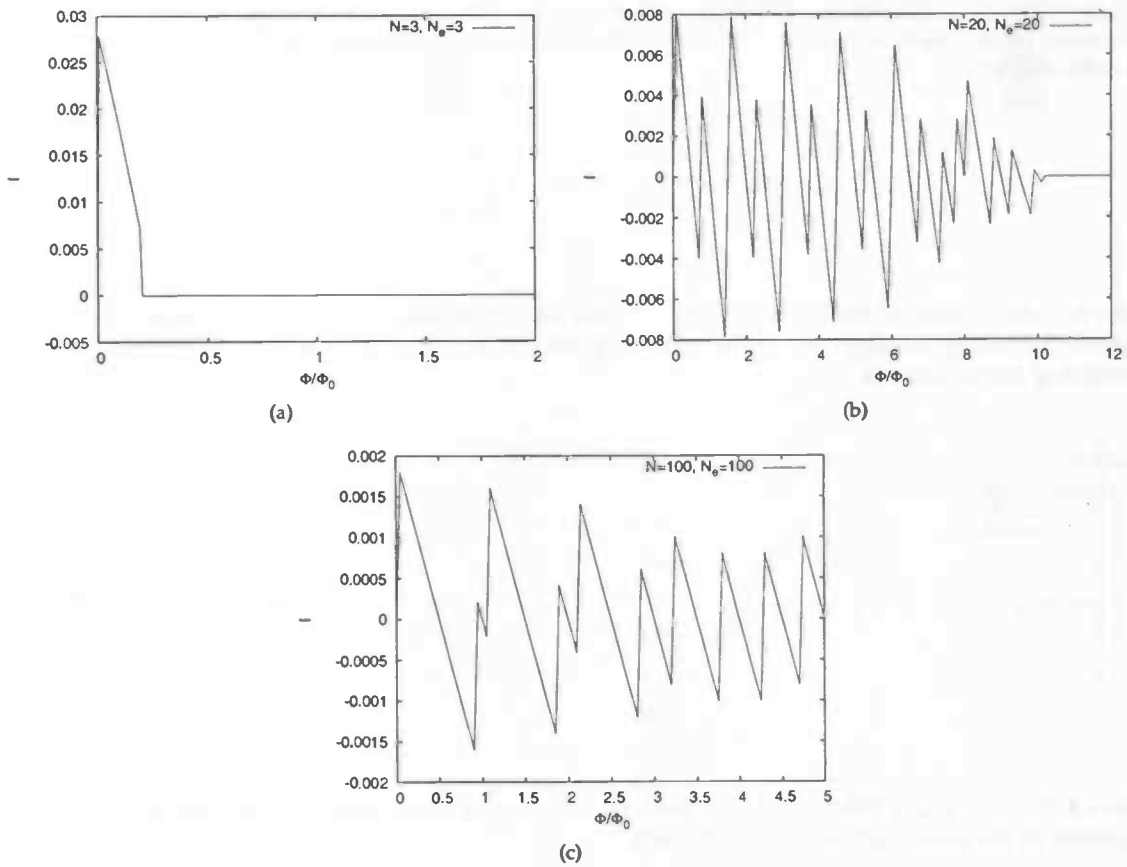

Figure 4.6: *Demonstration of the Zeeman effect, the current in the half-filled case with* $W = 0$ *as a function of* ϕ *for (a)* $N = 3$*, (b)* $N = 20$ *and (c)* $N = 100$.

4.4.2 Choice of the potential

In our first tight-binding approach all lattice points contain an atom and at each lattice site we assign a (random) potential. In effect the shape of this potential is rectangular, centered around the lattice sites, as shown in figure 4.7. In this section we mapped the continuous Hamiltonian onto our tight-binding Hamiltonian. In this situation we also have lattice points between the atoms. We now need to choose a potential shape. There are numerous choices we could make, for instance we could localize it at lattice sites containing an atom. This would in effect again be an "delta function" potential. However a "delta function" or rectangular potential does not seem a realistic model. Although the precise shape of the actual potential is unknown, a better choice seems to be an potential that is centered around the lattice sites containing an atom and decreases from there to a minimum in the middle of two atoms. The most simple potential of this kind is an triangular potential, with its extremum at the site containing an atom and is zero at the point halfway between two atoms like shown in figure 4.8. Even more realistic be a Gaussian shaped potential. We will use the the following potential as our Gaussian potential,

$$V(x) = \sum_i W_i e^{-25(\frac{x-x_i}{a})^2}, \tag{4.45}$$

where x_i is the location of the i'th atom. This potential has the feature that it is significant near the atom and nearly zero between atoms, as illustrated in Fig. 4.9 for $W_i = 1$.

We now demonstrate the effect of these potentials. In Figs. (a)-(d) we have plotted the average (dimensionless) persistent current at $\phi/\phi_0 = 0.25$ as a function of W. In order to make a fair comparison we

need to define the disorder strength W in such a way that the total "strength" of the disorder potential is the same for all potential shapes. Thus $\int V(x)dx$ is the same for all potentials. We define for the rest of this subparagraph[3],

$$W = \mathrm{Max}(W_i), \qquad W_i = \int_{x_i - a/2}^{x_i + a/2} dx[V(x)] \tag{4.46}$$

where x_i is the location of the i'th atom. Thus W now defines the maximum amount of work the random potential can do on an electron. In the following the averaging was done over 50 different random disordering configurations.

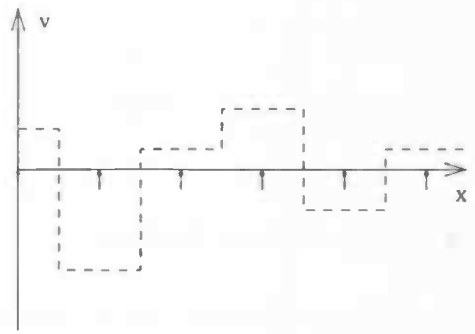

Figure 4.7: *Rectangular potential shape used implicitly in the initial tight-binding approach.*

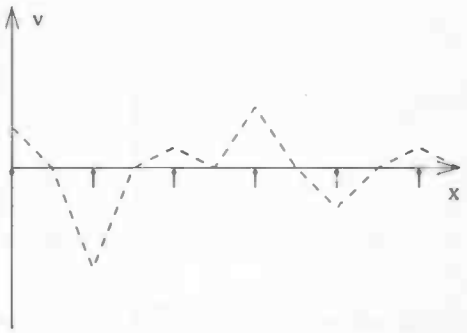

Figure 4.8: *A triangular shaped potential.*

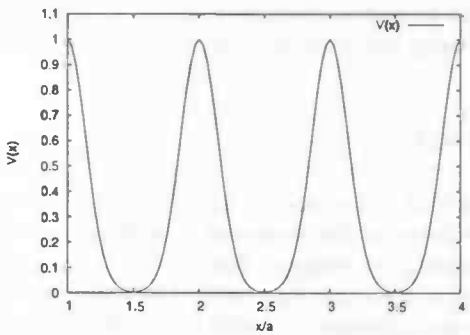

Figure 4.9: *The Gaussian function we use for our Gaussian shaped potential for $W = 1$, as defined in the text.*

Gold has a lattice constant $a \approx 0.5\lambda_f$. Thus in our calculations the localized potential with $\delta = 0.5$ corresponds to the tight-binding model. The results from the tight-binding approach differ greatly from the continuum values. This means that using our approach we will be able to do much more accurate calculations then was previously done. The persistent current for all three potentials converges for $\delta \to 0$, though the current is different in each potential as can be seen in figure 4.10(d). We found that the Gaussian potential is sampled accurately at $\delta = 0.1$. As this potential seems the most realistic we will use the Gaussian potential in our simulations.

[3]We will use this definition of W only in this subparagraph.

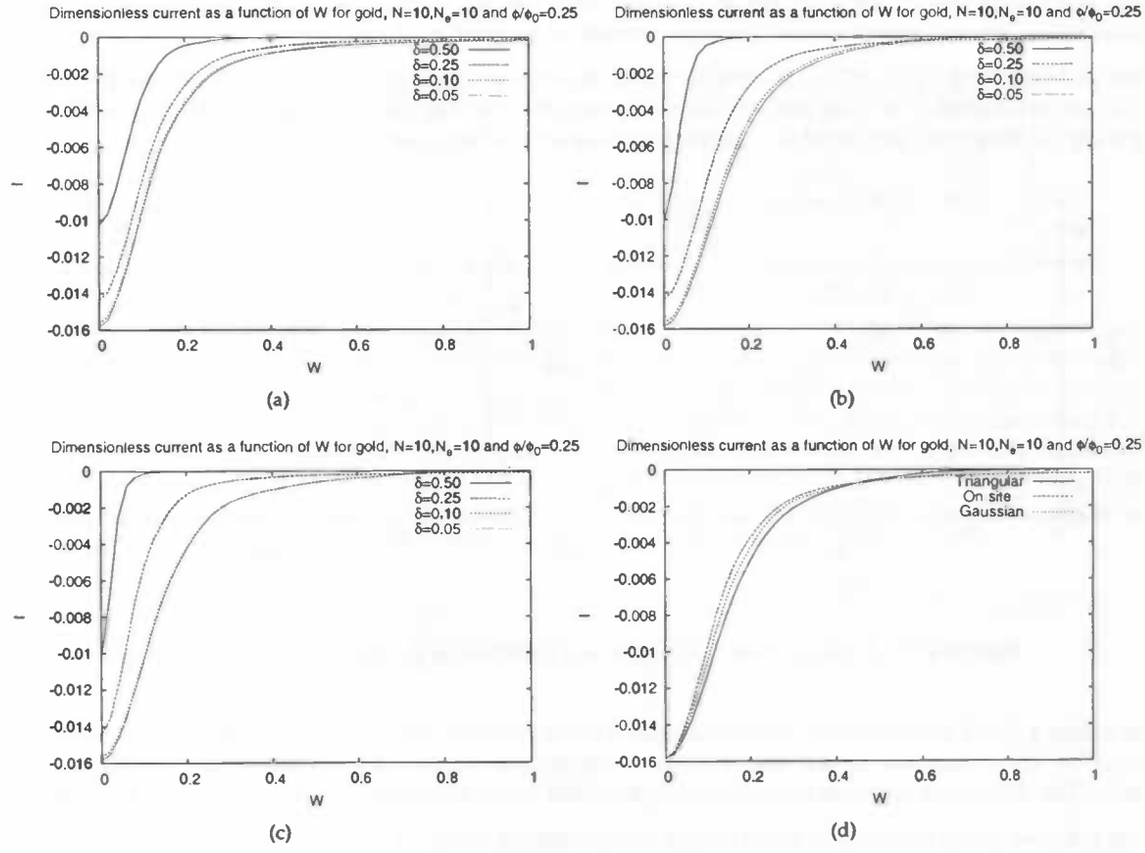

Figure 4.10: *Average current as a function of W with* $N = 10$ *and* $N_e = 10$ *for the following potentials: (a) The "localized potential" where the potential is only defined at sites containing an atom. (b) The triangular potential as shown in figure 4.8. (c) The Gaussian shaped potential defined by equation* (4.45). *(d) The three potentials together in one figure for* $\delta = 0.05$.

4.4.3 Numerical results

In section 2.5 we discussed the various persistent-current experiments. We will now try to reproduce these results with our numerical tool. Unfortunately the rings used in the experiments had of the order of 10^4 lattice sites. This is something which we can't simulate on an ordinary PC because we then would have to diagonalize an $10^4 \times 10^4$ Hamiltonian. The rings we will be considering are much smaller, nonetheless they should agree to considerable extent to experiment if all the important processes governing persistent currents are present in our system. In table 4.4.3 we list the basic properties of the materials used in these experiments, this serves as an input for our numerical work.

Metal	Valency	ρ_{el} [cm^{-3}]	k_f [cm^{-1}]	λ_f [cm]	v_f [cm s^{-1}]	E_f [eV]	Lattice spacing [Å]
Cu	1	8.45×10^{22}	1.36×10^8	4.62×10^{-8}	1.57×10^8	7.00	2.56
Au	1	5.90×10^{22}	1.20×10^8	5.23×10^{-8}	1.39×10^8	5.51	2.88

Table 4.1: *Basic properties of materials used in persistent current experiments, taken from Ref. [7]*

When we express the lattice spacing for gold and copper in terms of their Fermi wavelength we find that their lattice spacings are very similar. The lattice spacing of gold is 0.508023 [λ_f] and that of cop-

per is 0.554114 [λ_f]. In fact they are so close together that we cannot distinguish between them in our simulation. We will therefore use the same simulation for both gold and copper.

We will start with a ring of N = 20 sites and mesh size $\delta = 0.1$. In Figs. 4.11(a) and (a) we have plotted the current as a function of ϕ for various disorder strengths. Because the amplitude of the current depends greatly on the configuration of the disorder we take an average over 50 configurations.

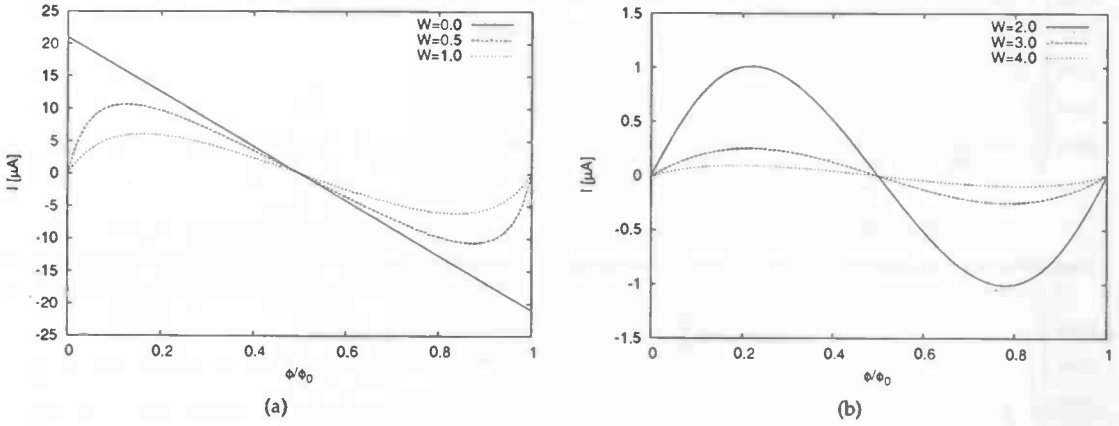

Figure 4.11: *Average current for gold as a function of ϕ, with N = 20 and $\delta = 0.1$.*

In tables 4.2 and 4.3 we present the amplitude of these currents. We have also indicated for which value of ϕ/ϕ_0 the maximum occurs. The results for copper are calculated from the results we obtained for gold. The difference between both current amplitudes is just the ratio between their Fermi energies.

We are now going to compare these results to experiment. For gold the expected current amplitude [8] is $0.3ev_f/L \leq I \leq 2.0ev_f/L$, giving, $2.31\,\mu A \leq I \leq 15.38\,\mu A$ is indeed consistent with our numerical results. With consistent we mean that the value of the current can be reproduced with a realistic value of W. For copper the expected current is [9][4] $I = 6 \times 10^{-3} ev_f/L = 0.29\,\mu A$. This is also consistent with our numerical results.

$W\,[E_f]$	$I\,[\mu A]$	$\phi_{max}\,[\phi_0]$
0.0	21.00	0.00
0.5	10.64	0.12
1.0	6.07	0.16
2.0	1.01	0.23
3.0	0.25	0.23
4.0	0.094	0.18
5.0	0.057	0.18

Table 4.2: *Current amplitudes for gold, with N = 20 and $\delta = 0.1$*

$W\,[E_f]$	$I\,[\mu A]$	$\phi_{max}\,[\phi_0]$
0.0	26.68	0.00
0.5	13.51	0.12
1.0	7.71	0.16
2.0	1.28	0.23
3.0	0.32	0.23
4.0	0.12	0.18
5.0	0.072	0.18

Table 4.3: *Current amplitudes for copper, with N = 20 and $\delta = 0.1$*

We will now repeat the previous calculations for N = 100. In this case we now cannot do an ensemble average over the entire range $0 \leq \phi/\phi_0 \leq 1$ because of the large amount of time needed for such a calculation (more than 24 hours for 50 averages over the entire range). Instead we do one calculation over a single disordering configuration and then calculate an average current at the maximum over 50 configurations.

In tables 4.4 and 4.5 we present the current amplitude for the various disordering strengths as well as

[4]The ensemble averaging has halved both the current and the amplitude of the current amplitude in this experiment. Thus to compare with our numerical values we need to add an factor two to their results.

the value of ϕ for which the maxima occur.

$W\ [E_f]$	$I\ [\mu A]$	$\phi_{max}\ [\phi_0]$
0.0	4.20	0.00
0.5	1.05	0.14
1.0	0.10	0.20
2.0	3.98×10^{-5}	0.25

Table 4.4: *Current amplitudes for gold, with* $N = 100$ *and* $\delta = 0.1$

$W\ [E_f]$	$I\ [\mu A]$	$\phi_{max}\ [\phi_0]$
0.0	5.34	0.00
0.5	1.33	0.14
1.0	0.13	0.20
2.0	5.06×10^{-5}	0.25

Table 4.5: *Current amplitudes for copper, with* $N = 100$ *and* $\delta = 0.1$

The experimental value of the current amplitude for gold is [8] $0.3\,\mu A \leq I \leq 3.06\,\mu A$ and that of copper is [9] $I = 6 \times 10^{-3} e v_f / L = 0.058\,\mu A$. We could argue that the numerical values are consistent with these experimental values in the sense that they agree for a realistic value of W. The current in the free electron case ($W = 0$) is expected to have an $1/L$ dependence in the current. Comparing the results for $N = 20$ and $N = 100$ we indeed see an factor 5. The currents for the cases with disordering however decrease much more rapidly. The experimental results on the other hand scale with $1/L$. This means that our model is unable to reproduce these experimental observations. Of course this is hardly surprising considering the simplicity of the model. Qualitatively there is good agreement.

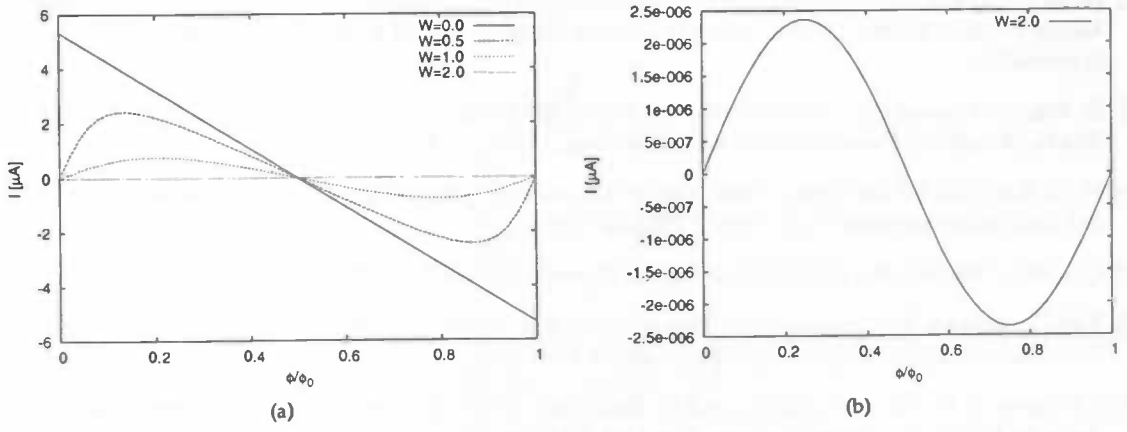

Figure 4.12: *Average current for gold as a function of* ϕ*, with* $N = 100$ *and* $\delta = 0.1$.

Bibliography

[1] G.D. Mahan, Many-particle physics, Plenum Publishers ISBN:0306463385 (2000).

[2] LAPACK, http://www.netlib.org/lapack/.

[3] H. de Raedt, *"Product formula algorithms for solving the time-dependent Schrödinger equation"*, Comput. Phys. Rep., 7, (1987), p.16

[4] H. de Raedt and W. von der Linden, *"Quantum lattice problems, The Monte Carlo Method in Condensed Matter Physics, Second Edition, Topics in Applied Physics"*, 71, ed K. Binder, Springer, (1995), p. 277 (appendix).

[5] D. Brink, *"Proceedings of the International School of Physics, Enrico Fermi"*, Course 36 (1965), ed. C. Bloch, (Academic Press, New York and London, 1966), p. 247.

[6] H. de Raedt and P. de Vries, *"Simulation of two and three-dimensional disordered systems: Lifshitz tails and localization properties"*, Z. Phys. B 77, 243(1989).

[7] C. Kittel, *"Introduction to Solid State Physics (Seventh Edition)"*, ISBN 0-471-11181-3.

[8] E.M.Q. Jariwala, P. Mohanty, M.B. Ketchen and R.A. Webb, *"Diamagnetic Persistent Current in Diffusive Normal-Metal Rings"*, Phys. Rev. Lett. 86 1594 (2001)

[9] L.P. Levy, G. Dolan, J. Dunsmuir and H. Bouchiat, *"Magnetization of Mesoscopic Copper Rings : Evidence for Persistent Currents."*, Phys. Rev. Lett. 64 2074 (1990)

Chapter 5

The quantum toy

5.1 Introduction

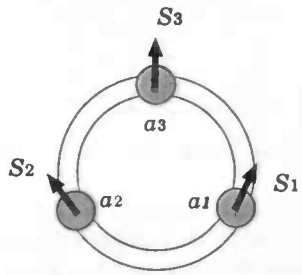

Figure 5.1: *The quantum toy, a metallic ring with three embedded ferromagnets. The direction of the magnetization is given by* $\vec{S}_i$.

Recently Tatara and Kohno [1] showed that a metallic ring containing three or more ferromagnets can carry an persistent current which is induced by the direction of the ferromagnets. In figure 5.1, such a ring with three ferromagnets is shown. In another paper Tatara and Garcia [2] proposed that this novel system (dubbed "the quantum toy") can perhaps be useful in the context of quantum computation.

An electron traversing a ring containing a number of ferromagnets will be scattered at each site containing a ferromagnet. At each scattering the wave function of the electron will be multiplied by a phase factor

$$A(\vec{n}_i) = \alpha e^{i\beta \vec{n}_i \cdot \vec{\sigma}}, \tag{5.1}$$

with α and β complex constants, n_i a unit vector along the magnetization direction and $\vec{\sigma}$ the Pauli spin matrices. The scattering will induce a different phase shift for electrons moving clockwise than those moving counter-clockwise. The reason for this is that the Pauli spin matrices do not commute. Thus, for a ring containing *two* ferromagnets we have a phase difference

$$\Delta = A(\vec{n}_1)A(\vec{n}_2) - A(\vec{n}_2)A(\vec{n}_1) \neq 0. \tag{5.2}$$

Charge transport however arises from the trace of the phase shift[1]. Since

$$\mathrm{Tr}(A(\vec{n}_1)A(\vec{n}_2)) - \mathrm{Tr}(A(\vec{n}_2)A(\vec{n}_1)) = 0, \tag{5.3}$$

as can be easily deduced from the Pauli matrix commutator,

$$[\sigma_i, \sigma_j] = 2i\epsilon_{ijk}\sigma_k, \tag{5.4}$$

with ϵ_{ijk} the Levi-Cevita tensor. We will need at a minimum three ferro magnets. Using the fact that

$$e^{i\beta\sigma_i} = \cos(\beta) + i\sigma_i \sin(\beta) \tag{5.5}$$

we find the current I to be proportional to

$$I \propto \mathrm{Tr}(A(\vec{n}_1)A(\vec{n}_2)A(\vec{n}_3)) - \mathrm{Tr}(A(\vec{n}_3)A(\vec{n}_2)A(\vec{n}_1)) = 4\alpha^3 \sin^3(\beta)\vec{n}_1 \cdot (\vec{n}_2 \times \vec{n}_3). \tag{5.6}$$

Thus when there are three ferromagnets embedded in the ring a current can be induced and the amount of current depends on the direction of the ferromagnets. For more then three spins the problem will rapidly become more complicated. As all the basic features are present in the case of three magnets we will focus on that.

The product $\vec{n}_1 \cdot (\vec{n}_2 \times \vec{n}_3)$ can only be non zero when none of ferromagnets are parallel to each other. It is this fact that gives the quantum toy its interesting features. Suppose we fix one of the ferromagnets in a certain direction and define that direction to be the $\hat{z}$ direction. We put the other two spins in the x-y plane. The product in (5.6) can only be non zero if one spin is in the $\hat{x}$ direction and the other in $\hat{y}$ direction. We now assign a value to both directions, we assign the value 0 to the $\hat{x}$ direction and assign 1 to the $\hat{y}$ direction. We can now study when a current I is induced in this scheme by creating a truth table for $C = \hat{z} \cdot (\vec{n}_2 \times \vec{n}_3)$ as shown in Table 5.1

S_2	S_3	C
0	0	0
0	1	1
1	0	-1
1	1	0

Table 5.1: *Truth table of* $C = \hat{z} \cdot (S_2 \times S_3)$, *with* $0 = \hat{x}$ *and* $1 = \hat{y}$.

From Table 5.1 we conclude that the quantum toy operates like a CNOT(XOR) gate. As we saw in the first chapter the CNOT gate is a fundamental port for quantum computation. At first sight this looks very promising. Unfortunately it turns out that the gate is not suitable for quantum computation. To use the gate in a quantum circuit we need to transfer the output of a first gate α (the output being the existence of a current) onto a second ring β. We could of course inject the current onto a second ring but this is not sufficient. To couple both CNOT gates, we have to couple existence of a current on the first ring α to the direction of one of the ferromagnet on ring β. This however is not something that can be done in a way that is useful for quantum computation.

Another way to view the quantum toy is to view the ring itself as a qubit. We call the state where the ring carries a current 1 and the state without a current 0. It is is unclear however how such a qubit could be used in a way relevant for quantum computation.

A more useful application is perhaps to use the quantum toy as a high precision magnetic field measurement device. By aligning one spin along the field to be measured we could by manipulating the direction of the other two spins[1] observe the direction of the magnetic field by observing the induced current. This of course can only be done if the response of the current to the variation of the ferromagnets is large enough to obtain a sufficient sensitivity.

The perturbation theory of Tatara and Kohno[1] yields the induced current density in a ring with three ferromagnets (for temperature $T = 0$):

$$j = -\frac{2ev_F}{L}\left(\frac{J}{\epsilon_F}\right)^3 \cos(k_F L)\,\vec{n_1}\cdot(\vec{n_2}\times\vec{n_3}), \tag{5.7}$$

where $v_F = \hbar k_F/m$ is the Fermi velocity, $J \equiv \pi W\Delta/L$ with L the length of the ring, W the width of the ferromagnets and Δ the coupling strength between the ferromagnets and electrons traversing the ring.

[1] Typically we would fix one spin and vary the other.

In the following chapter we will simulate a quantum toy system using the simulation tool developed in the previous section, we will test the validity of equation (5.7) and explore the possibility to use the quantum toy as an measurement device.

5.2 Numerical simulations

Tight binding model calculations

For simplicity we will start with a tight-binding approach, which is sufficient to obtain the qualitative features of the system. Later when we are going to do more quantitative calculations we shall parametrize the Hamiltonian to make contact with the continuum model, similarly to what we did in section 4.4. The tight-binding model for a system with embedded ferromagnets is

$$H = -t_0 \sum_i \sum_\sigma (c^\dagger_{i,\sigma} c_{i+1,\sigma} + c^\dagger_{i+1,\sigma} c_{i,\sigma}) + C \sum_i \sum_j \hat{c}^\dagger_i \vec{\sigma} \cdot \vec{n}_j \hat{c}_i + \sum_i W_i n_i, \tag{5.8}$$

where $C \propto \Delta$ is a coupling constant, n_i the counting operator, $\hat{c}_i = \begin{pmatrix} c_{i,\uparrow} \\ c_{i,\downarrow} \end{pmatrix}$ and $\vec{n}_j$ is the magnetization direction of the j'th ferromagnet. For the Suzuki-Trotter decomposition we choose to split the Hamiltonian in two parts

$$A = -t_0 \sum_i \sum_\sigma (c^\dagger_{i,\sigma} c_{i+1,\sigma} + c^\dagger_{i+1,\sigma} c_{i,\sigma}), \qquad B = C \sum_i \sum_j \hat{c}^\dagger_i \vec{\sigma} \cdot \vec{n}_j \hat{c}_i + \sum_i W_i n_i. \tag{5.9}$$

The current operator associated with this Hamiltonian is the same as in the previous case, which we will now prove. The current operator is defined by $j = i[H, P]$. Of course to see how the current operator changes we only need calculate the commutator for the terms concerning the ferromagnets, thus we only need to calculate, $[\hat{c}^+_i(\vec{\sigma} \cdot \vec{n})\hat{c}_i, \hat{c}^+_j \hat{c}_j]$. To simplify notation we substitute $A = \vec{\sigma} \cdot \vec{n}$. Because creation/annihilation working on different lattice sites always commute we can drop the particle index, we can now evaluate the commutation relation

$$[\hat{c}^+_\sigma A_{\sigma\sigma'} \hat{c}_{\sigma'}, \hat{c}^+_s \hat{c}_s] = A_{\sigma\sigma'}[\hat{c}^+_\sigma \hat{c}_{\sigma'}, \hat{c}^+_s \hat{c}_s - \hat{c}^+_s \hat{c}_s \hat{c}^+_\sigma \hat{c}_{\sigma'}] \tag{5.10}$$

This can only be non zero when $s = \sigma$ or $s = \sigma'$, thus the commutator becomes

$$A_{\sigma\sigma'}[\hat{c}^+_\sigma \hat{c}_{\sigma'} \hat{c}^+_\sigma \hat{c}_\sigma - \hat{c}^+_\sigma \hat{c}_\sigma \hat{c}^+_\sigma \hat{c}_{\sigma'} + \hat{c}^+_\sigma \hat{c}_{\sigma'} \hat{c}^+_{\sigma'} \hat{c}_{\sigma'} - \hat{c}^+_{\sigma'} \hat{c}_{\sigma'} \hat{c}^+_\sigma \hat{c}_{\sigma'}]. \tag{5.11}$$

Applying the fermionic commutation relations to this result gives

$$A_{\sigma\sigma'}[\hat{c}^+_\sigma(\delta_{\sigma\sigma'} - \hat{c}^+_\sigma \hat{c}_{\sigma'})\hat{c}_\sigma - \hat{c}^+_\sigma(1 - \hat{c}^+_\sigma \hat{c}_\sigma)\hat{c}_{\sigma'} + \hat{c}^+_\sigma(1 - \hat{c}^+_{\sigma'} \hat{c}_{\sigma'})\hat{c}_{\sigma'} - \hat{c}^+_{\sigma'}(\delta_{\sigma\sigma'} - \hat{c}^+_\sigma \hat{c}_{\sigma'})\hat{c}_{\sigma'}], \tag{5.12}$$

which simplifies to

$$A_{\sigma\sigma'}[\delta_{\sigma\sigma'} \hat{c}^+_\sigma \hat{c}_\sigma - \hat{c}^+_\sigma \hat{c}_{\sigma'} + \hat{c}^+_\sigma \hat{c}_{\sigma'} - \delta_{\sigma\sigma'} \hat{c}^+_{\sigma'} \hat{c}_{\sigma'}] = 0, \tag{5.13}$$

thus the current operator remains unchanged.

Now we start by testing the time step operator for a ring of N sites. We insert 3 spins which are distributed equally over the ring. We put the first spin in the $\hat{x}$ direction, the second in the $\hat{y}$ direction and the third in the $\hat{z}$ direction[2]. We can verify the results of the time step operator by comparing them to results obtained by diagonalizing the Hamiltonian directly with LAPACK. In Figs. 5.2(a)-(d)we plot the error on the wave function for various values of N and τ. We use $\phi = 0.25$, $W = 1$ and $C = 1$.

[2]From now on we will use the notation $(\hat{x}, \hat{y}, \hat{z})$ for such an arrangement.

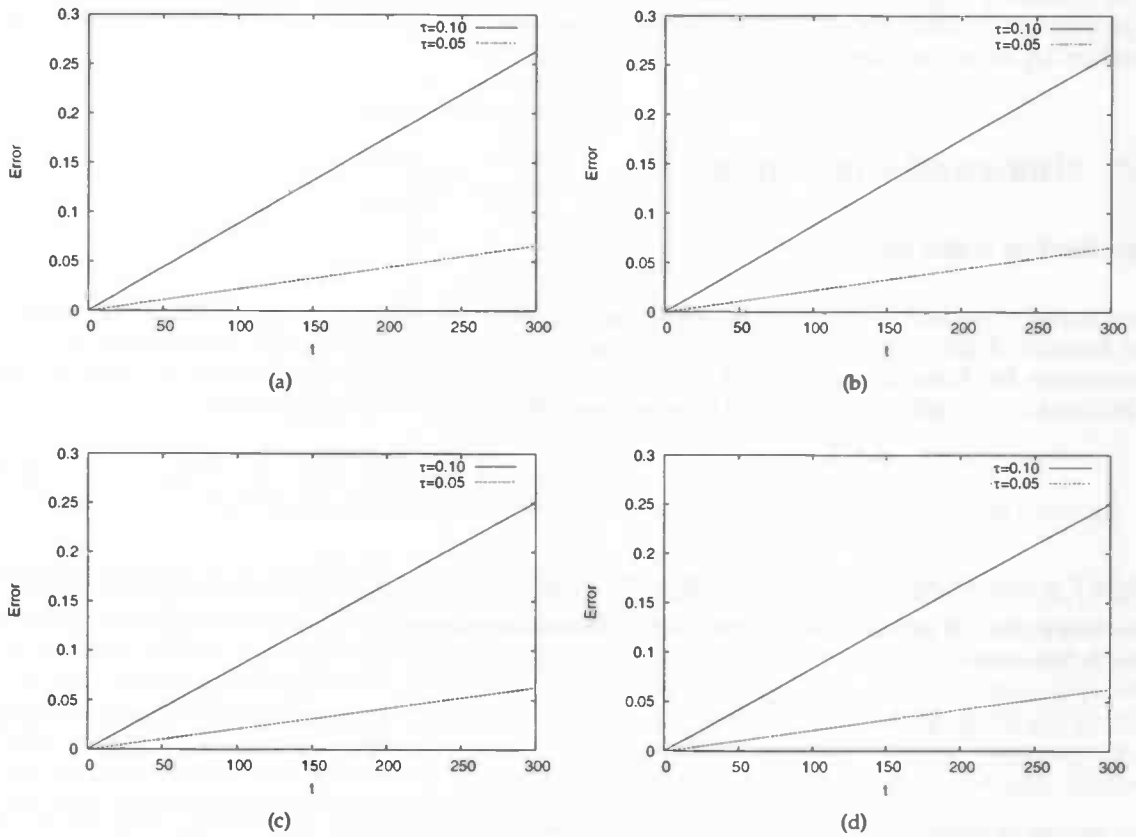

Figure 5.2: *Error in time step operator for (a)* $N = 3$*, (b)* $N = 4$*, (c)* $N = 99$ *and (d)* $N = 100$

There is a factor 4 between the error for $\tau = 0.1$ and $\tau = 0.05$. This is consistent with the expected quadratic convergence of the second order Suzuki-Trotter method. Thus we can be confident that our simulation code is working properly. We will now show that the expected relation between the direction of the ferromagnets and the current, $I \propto \vec{n_1} \cdot (\vec{n_2} \times \vec{n_3})$, is indeed observed in our simulation. In figures 5.3(a)-(d) we plot the current as a function of the electron density for a number of spin configurations, we use $C = 0.05$ in all cases. For the configuration of magnetization direction of Figs. 5.3(c) and (d) we expect that the current is zero and indeed, the numerical data confirms this. In cases carrying a current we observe that the size of current fluctuates wildly with the electron density. The current even becomes zero for configurations that according to theory[1] should carry a current. For example when N is even then the current is zero at $N_e = N/2$. This effect will disappear when we go to the continuum case. The conclusion therefore is that we can use the tight-binding model for one electron to simulate the qualitative features of a quantum toy, but for the many-electron case we need to go to the continuum model.

We now need to investigate the dependence of the current on the coupling constant C. The ferromagnets have a sort of double effect. On the one hand they can in the right configurations induce a persistent current. But on the other hand electrons also scatter from the ferromagnets which actually reduces the current. In Fig. 5.4 we plot the current as a function of C with $W = 0$ and the ferromagnet configuration $(\hat{x}, \hat{y}, \hat{z})$.

The interplay between both effects is clearly visible. According to theory[1] the current should scale with C^3 for small[3] C (see (5.7)). However when we magnify the response for small C we find that the current

[3]Equation (5.7) was derived using perturbation theory, so we can only expect it to hold for small C

is proportional to C^2 for small C. As we are not in the continuum limit we cannot necessarily expect that (5.7) will hold, therefore statements about the correctness of (5.7) have to be postponed until the next subsection.

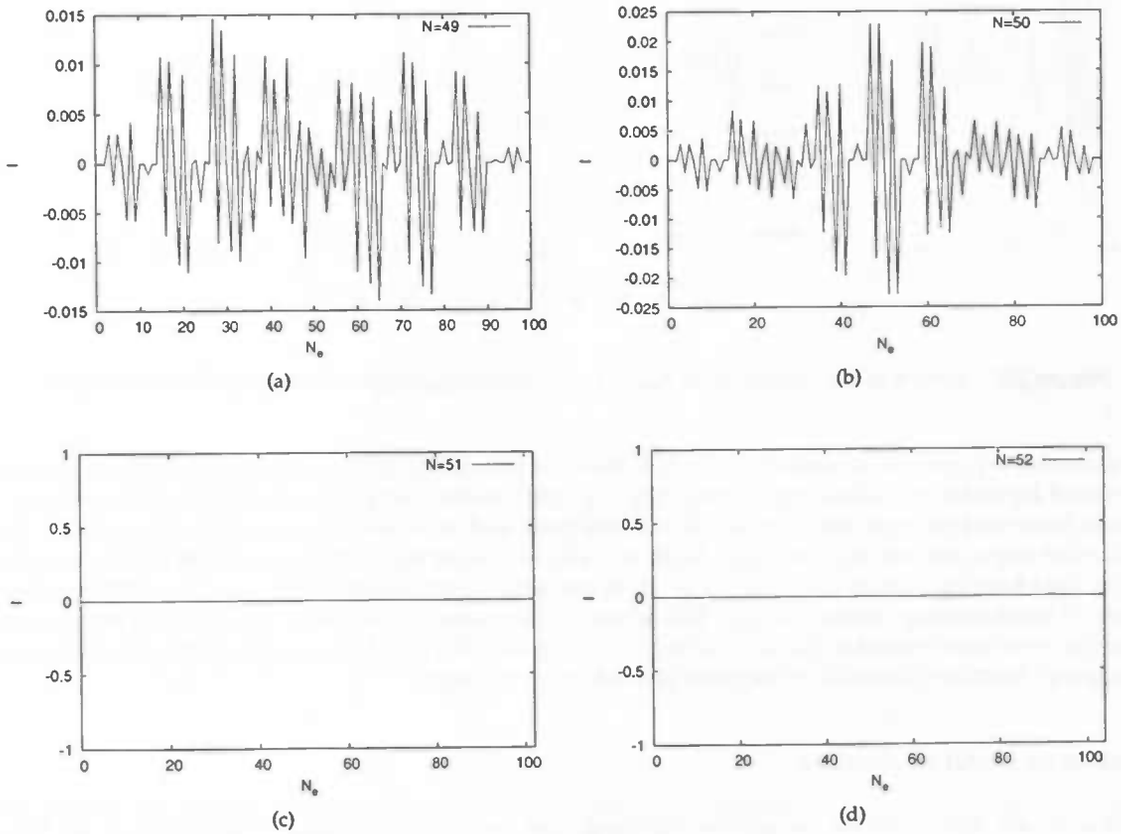

Figure 5.3: *The current as a function of* N_e *for spin configurations (a)* $(\hat{x},\hat{y},\hat{z})$*, (b)* $(\hat{x},\hat{y},\hat{z})$*, (c)* $(\hat{x},\hat{x},\hat{z})$ *and (d)* $(\hat{y},\hat{y},\hat{y})$.

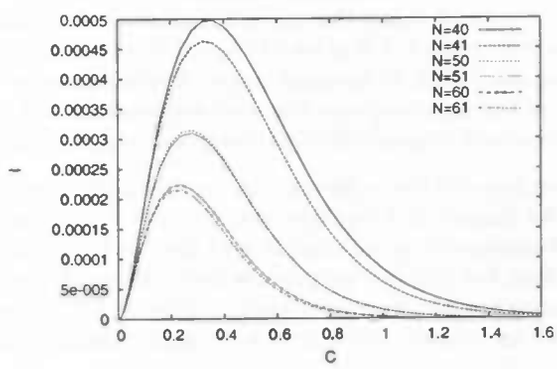

Figure 5.4: *Current as a function* C *for* $N_e = 1$ *and spin configuration* $(\hat{x},\hat{y},\hat{z})$.

To conclude our numerical study of the single electron case we show the N dependence of the current. In Fig. 5.5 we plot the N dependence for $N_e = 1$, $C = 0.05$, $W = 0$ and ferromagnet configuration $(\hat{x},\hat{y},\hat{z})$. The current scales with $\sqrt{N}$, not at all what we would be expect from (5.7), which predicts that the current scales as $1/N^4$. But as we already noted, we do not necessarily expect (5.7) to hold in this

system. The current as a function of N is well behaved in the sense that for larger rings one extra lattice site yields only a small change of the current.

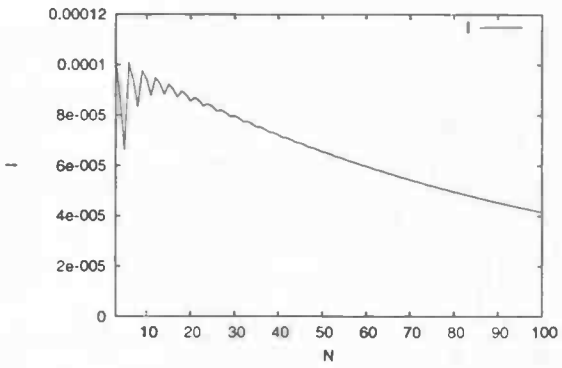

Figure 5.5: *Current as a function* N *for* $N_e = 1$, *we use spin configuration* $(\hat{x}, \hat{y}, \hat{z})$ *and* $C = 0.05$.

As a concluding remark we would like to note that it is possible to build such a single electron system. We could for instance make a conducting ring of a small number of molecules [3]. For this system we would have controll over the number of free electrons and thus be able to enforce $N_e = 1$. In this molecular ring quantum toy it will also be more valid to use the tight-binding method than in a metal. In the tight-binding picture electrons "hop" from one atom to the other, but in a real metal the electron shells of neighbouring atoms overlap. This is one of the main reasons why we will map our system onto the continuum model in the next subsection. In a molecular ring however the notion of an electron "hopping" from one molecule to the other is much more realistic.

Continuum model calculations

Similar to our discussion for the spatial distribution of the on-site potential in section 4.4.2, we have to model the strength of the ferromagnets in space. Because of the highly localized nature of magnetic impurities we will use a delta function potential (i.e. the ferromagnets are localized at sites containing an atom). In Figs. 5.6(a)-(d) we plot the current as a function of the electron density for a number spin configurations. We use $C = 0.05$ in all cases. The current has been calculated using the parameters for gold, allowing us to scale the y-axis in μA. 5.7(a) and (b) we plot the current as a function of C for $W = 0$ and the ferromagnet configuration $(\hat{x}, \hat{y}, \hat{z})$ for gold rings. Observe that the qualitative features of the dependence of the current on the ferromagnets direction are present, but that the N_e dependence is quite erratic. This kind of behaviour is clearly in violation to what is predicted by equation (5.7).

We now investigate the dependence of the current on the coupling constant C in the continuum case. In Figs. 5.7(a) and (b) we plot the current as a function of C for $W = 0$ and the ferromagnet configuration $(\hat{x}, \hat{y}, \hat{z})$ for gold rings. The behaviour is more complicated than in the tight-binding case. For example there is a strong even-odd effect. For odd N the current is three orders of magnitude larger than for even N. Also there is a discontinuous jump in the current at $C = 0$ for odd N. Though for the case of even N, the current does scale with C^3 for small C, we again have found a violation of equation (5.7).

We are now going to study the N dependence of the current. Previously we found that there was a strong even-odd effect, therefore we will study the case of odd and even N separately. In Figs. 5.8(a) and (b) we plot the N dependence for gold rings. We will use the ferromagnet configuration $(\hat{x}, \hat{y}, \hat{z})$, $W = 0$ and take $\delta = 0.1$ for the mesh size.

According to equation (5.7) the current should scale as $1/N^4$. Neither for even N or odd N this is the case. Surprisingly the shape of the current as a function of the lattice size is a damped periodic signal with a periodicy of 12 sites, for which unfortunately we presently have no explanation. Another striking feature

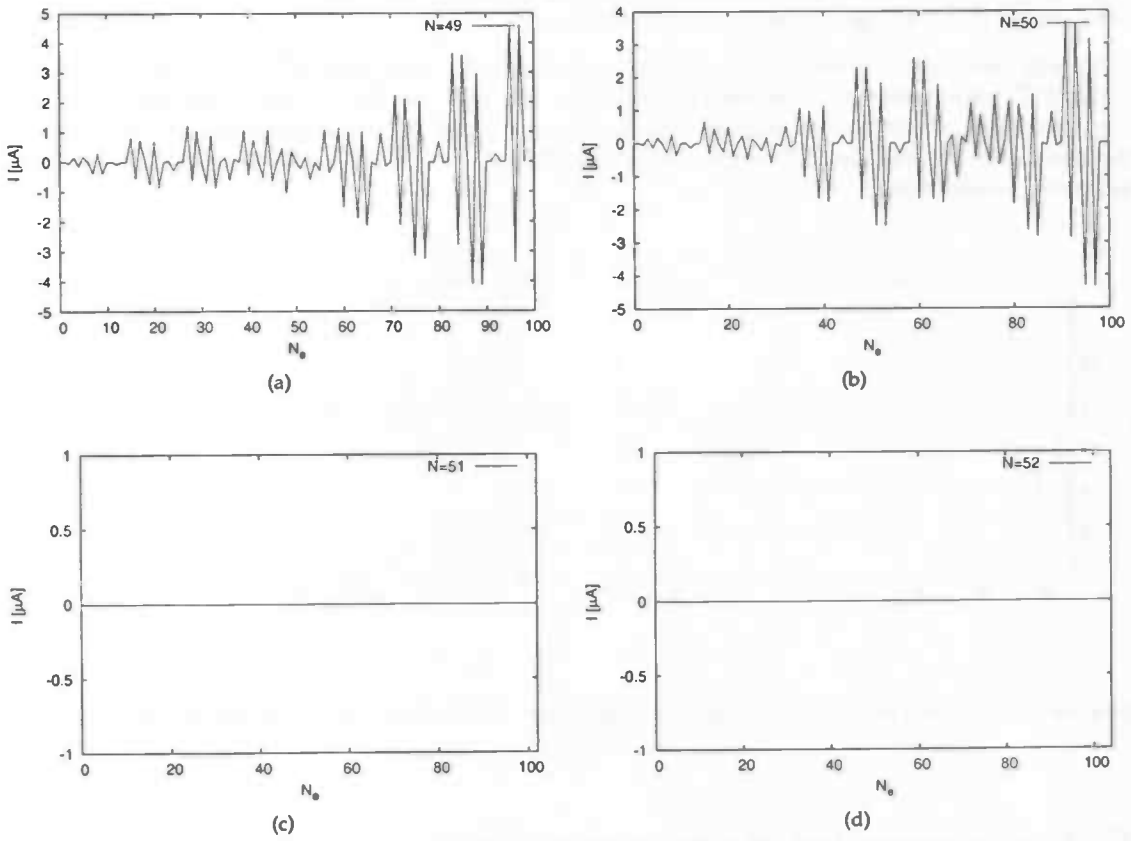

Figure 5.6: *The current as a function of* N_e *for spin configurations (a)* $(\hat{x},\hat{y},\hat{z})$*, (a)* $(\hat{x},\hat{y},\hat{z})$*, (a)* $(\hat{x},\hat{x},\hat{z})$ *and (a)* $(\hat{y},\hat{y},\hat{y})$*.*

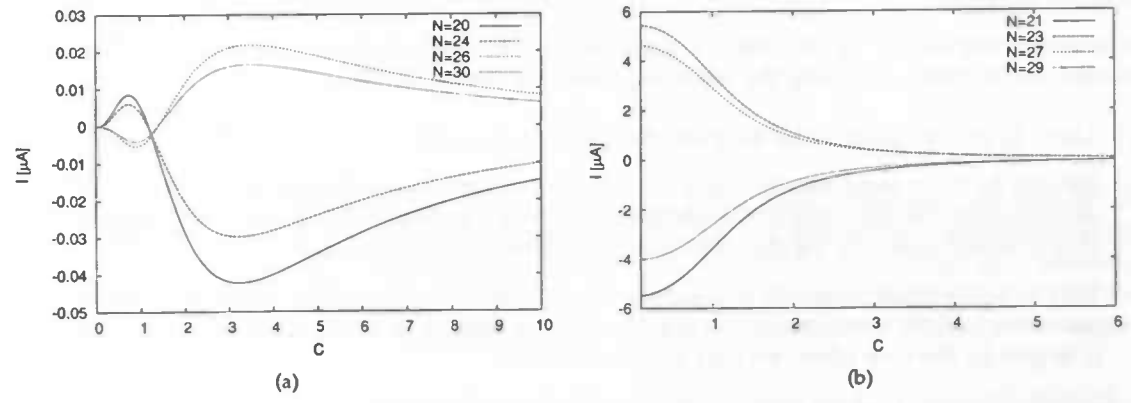

Figure 5.7: *Current as a function* C *for gold for spin configuration* $(\hat{x},\hat{y},\hat{z})$ *with (a)* $N = even$ *and (b)*$N = odd$*.*

is that the current for odd N is three orders of magnitude larger then when N is even. The explanation for this lies in the C dependence of the current, as can be seen in Figs. 5.7(a) and (b). Needless to say, the N dependence of the current is far from well behaved. Meaning that a small increase in the number of lattice sites can make a large difference in the current.

We can only conclude that we are not able to reproduce (5.7). It is possible that in the derivation of equation (5.7) not all relevant terms were included. For instance, perhaps the scattering effect due to the ferromagnets was not taken into account. We can unfortunately not check which effects were included in the derivation of equation (5.7) without repeating the calculation. This unfortunately is beyond the scope of this master thesis.

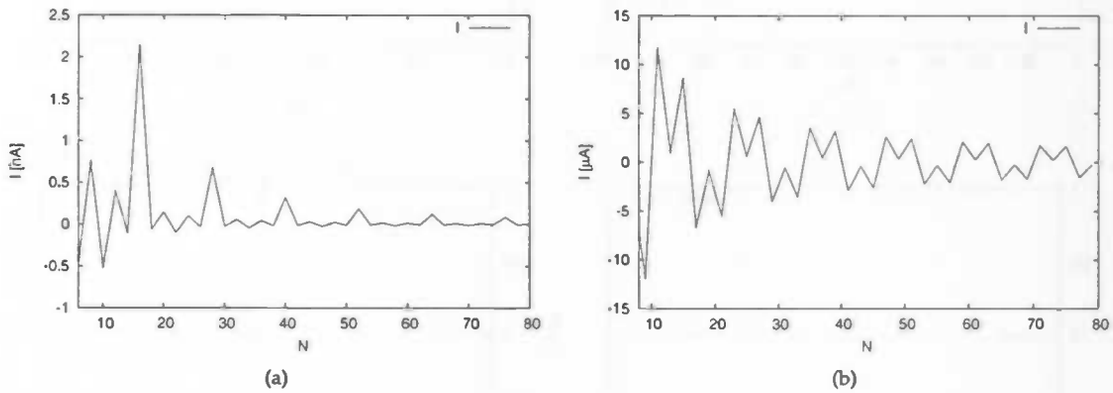

(a) (b)

Figure 5.8: *Current as a function* N *for spin configuration* $(\hat{x}, \hat{y}, \hat{z})$ *and* $C = 0.1$ *in gold for (a) even* N *and (b) odd* N.

5.3 The quantum toy as a measuring device

Even though we cannot reproduce (5.7) quantitatively in our simulation, we have observed the $I \propto \vec{n_1} \cdot (\vec{n_2} \times \vec{n_3})$ dependence of the current. Therefore it might still be possible to use the quantum toy as a measuring device of the type we discussed in section 5.1. We found in the previous section that the single electron case was well behaved, therefore a single electron molecular ring as discussed in the previous section would be the most logical candidate. For completeness however we will also consider the case of gold rings.

The measurement device we propose is a quantum toy with three ferromagnets S_1, S_2 and S_3, a measurement can be conducted using the following three step measurement procedure.

Step 1 Allow S_1 to align itself to the magnetic field to be measured.

Step 2 Initially fix S_2 in some direction and vary S_3 in the plane perpendicular to S_2. By observing the magnitude of the induced current we can put S_3 perpendicular to the plane containing S_1 and S_2. This direction is simply the direction where the current is a maximum.

Step 3 Vary S_2 in the plane perpendicular to S_3 to find the direction of S_1. Here we have two options, we can either look for a maximum or a minimum in the current, as we shall see shortly the sensitivity is largest for the case where we look for a minimum

For this scheme to work there needs to be a sufficient sensitivity of the current on the direction of the ferromagnets. To show the sensitivity we put the ferromagnets in the configuration $(\sqrt{1-\gamma^2}\hat{x}+\gamma\hat{y}, \hat{y}, \hat{z})$ and then plot the current for $0 \leq \gamma \leq 1$. In effect we rotate the first spin from the $\hat{y}$ direction to the $\hat{x}$ direction. The results are presented in Figs. 5.9(a)-(c).

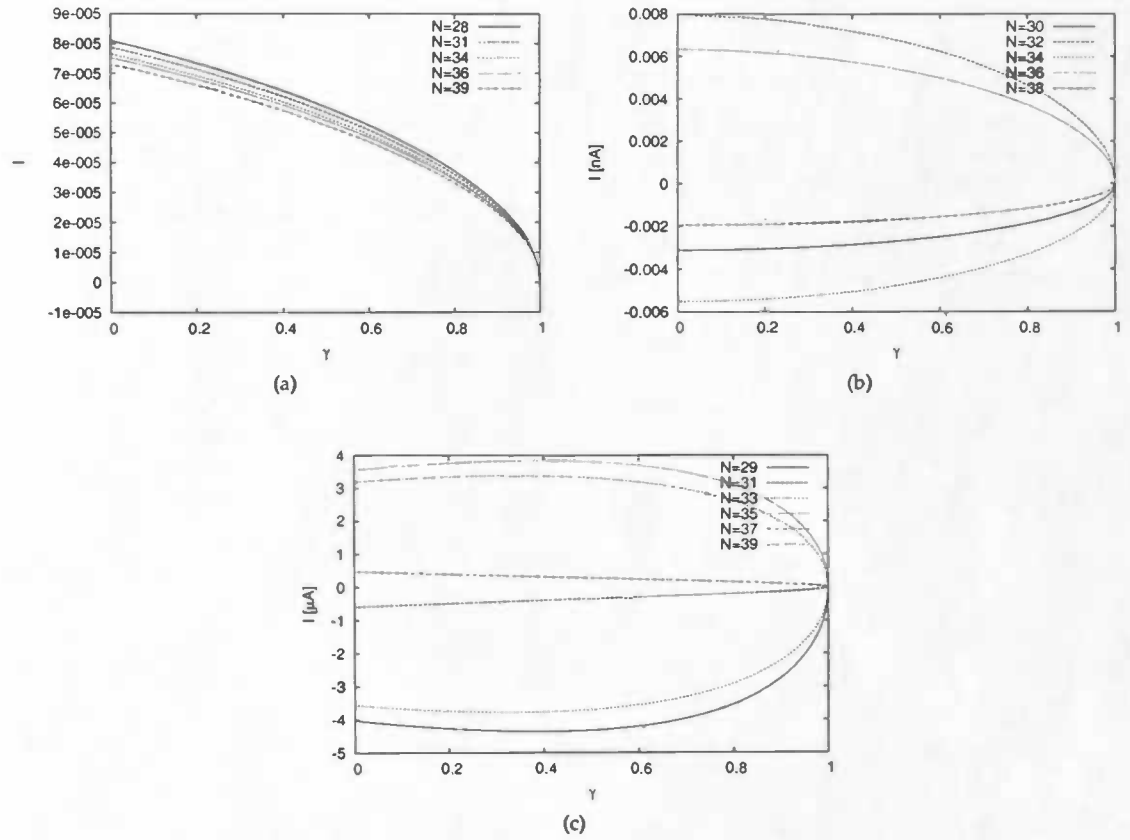

Figure 5.9: *Angular dependence of current for spin configuration* $(\sqrt{1-\gamma^2}\hat{x} + \gamma\hat{y}, \hat{y}, \hat{z})$ *and* $C = 0.05$ *in (a) single electron rings, (b) gold rings* ($N_e = N$) *with even* N *and (c) gold rings* ($N_e = N$) *with odd* N.

In the single electron case we observe indeed the $I \propto \vec{n_1} \cdot (\vec{n_2} \times \vec{n_3})$ behaviour. The angular dependence is largest around the minimum but is also sizable around the maximum. In the case of the gold rings we see that for odd N the maximum is *not* always at $\gamma = 0$. As we will not be able to choose the exact number of lattice sites in a gold ring, we will be unable to perform *step two* of the measurement procedure. Therefore according to our simulations this kind of scheme will only work for a molecular ring type quantum toy.

5.4 Conclusion

The reason we became interested in the quantum toy is the simple relation between the current I and the direction of the embedded ferromagnets, namely $I \propto \vec{n_1} \cdot (\vec{n_2} \times \vec{n_3})$. This relation between the current and the ferromagnet direction makes the quantum toy a natural XOR port, which led us to investigate the possibility to use the quantum toy as a candidate for quantum computer hardware. Unfortunately our analysis in the first section showed that the quantum toy was not suitable for quantum computer hardware.

As a second application we proposed that it would be possible to exploit the $I \propto \vec{n_1} \cdot (\vec{n_2} \times \vec{n_3})$ dependence to use the quantum toy as a measurement device. This was only possible if the current is given by (5.7),

$$j = -\frac{2ev_F}{L}\left(\frac{J}{\epsilon_F}\right)^3 \cos(k_F L)\, \vec{n_1} \cdot (\vec{n_2} \times \vec{n_3}). \tag{5.14}$$

We checked the validity of equation (5.7) numerically for two different system. The first system was a single electron tight-binding system. Here we would not expect (5.7) to hold quantitatively. We however found the most important qualitative feature, namely the $I \propto \vec{n_1} \cdot (\vec{n_2} \times \vec{n_3})$ dependence. We concluded that such a system could be used as a measurement device.

The second system was a gold ring, here we found large deviations from (5.7). There is a large even-odd effect. The current is three orders of magnitude larger for a ring with an odd number of lattice sites then it is for a ring of an even number of sites. Also for a ring with an odd number of sites, $I \propto \vec{n_1} \cdot (\vec{n_2} \times \vec{n_3})$ is not fulfilled. We were therefore unable to reproduce (5.7) and according to our calculations a metallic ring type quantum toy would be unsuitable as a measurement device. The reason for the deviation between theory and our calculations remains unclear.

Bibliography

[1] G. Tatara and H. Kohno, *"Permanent current from noncommutative spin algebra"*, Phys. Rev. B **67**, 113316 (2003).

[2] G. Tatara and N. Garcia, *"Quantum Toys for Quantum Computing: Persistent Currents Controlled by the Spin Josephson Effect"*, Phys. Rev. Lett. **91**, 076806 (2003).

[3] S. Miyashita, private communication.